LOCAL VARIABILITY IN EARLY OLIGOCENE PALEOSOLS AS A RESULT OF ANCIENT SOIL CATENARY PROCESSES, BRULE FORMATION, TOADSTOOL PARK, NEBRASKA

A Thesis

Submitted to

The Temple University Graduate Board

In Partial Fulfillment

Of the Requirements for the Degree

MASTER OF SCIENCE

By

Raymond C. Kennedy

May 2011

Dr. Dennis O. Terry, Jr., Advisor

Dr. David E. Grandstaff

Dr. Allison Tumarkin-Deratzian

ABSTRACT

Paleopedology is often employed in paleoenvironmental reconstructions because the features of paleosols are affected by changes in climate, ecology, topography, and lithology over time. These changes cause small-scale variations in the morphology and apparent development of paleosols and influence the degree to which certain soil features are preserved in the rock record. When drawing inferences about paleoenvironments based on paleosols, care must be taken to ensure that as many of the soil forming factors as possible are understood. Whereas climates can be ignored over small areas, and lithology represents the medium of soil preservation, topographic relief can vary dramatically over local scales, thereby influencing the partitioning of plant communities and contributing greatly to the development of soils. In this study, paleo-geomorphological relationships were investigated along a paleovalley sequence in the Early Oligocene Orella Member of the Brule Formation in the White River Group of Toadstool Park, NE. A series of three separate, but laterally contiguous, soil profiles exhibit variation in the type and degree of apparent pedogenesis. Changes in the presence, abundance, and size of soil features, such as root traces and soil structure, were observed over a distance of ~350 meters. The morphology and mineralogy of the soils along this paleovalley varied according to those processes which are influenced by paleotopography. Geochemical proxies of soil processes, as well as soil micromorphology, indicate only weak pedogenesis. This limited the utility of geochemical climofunctions used in the study, which were not found to differ significantly between geomorphological positions.

DEDICATION

This project is dedicated to the memory of my late father, Raymond P. Kennedy, who inspired and encouraged my interest in the natural world. His determination and persistence continue to inspire me, and I hold his achievements as a measure against my own. I love you, Dad.

ACKNOWLEDGEMENTS

This project was supported by Challenge Cost Share Agreement 05-PA-11020700 to Dr. Dennis O. Terry Jr. (DT) from the United States Forest Service, with the logistical assistance of Barbara Beasley. The inspiration for this project was the fruit of the many enjoyable discussions with my advisor, DT. His interdisciplinary interest in soils is what brought me to Temple University in the first place. I would also like to mention Mr. David Lane, Dr. Randal Miles, and Dr. Kenneth Macleod, who led me on my gradual path toward paleopedology. The mountain of paperwork and bureaucracy, which stood between me and the culmination of my time at Temple University, could not have been scaled without the dedication and kindness of Shelah Cox.

The critical assessment of my work provided by my committee members, Dr. David Grandstaff and Dr. Allison Tumarkin-Deratzian, and by Dr. George Myer and the other faculty in the Department of Earth and Environmental Sciences, is greatly appreciated, and has contributed to the quality of this project, as has the help of Dr. Stan Mertzman from the X-ray Laboratory at Franklin and Marshall College.

The cooperation and support of my peers, notably Stephen Peterson, Neil Griffis, Jesse Thornburg , Bill Lukens, Ed Welsh, and Sarah Lyter, in both the field and in the laboratory and by intellectual exchange, helped to maintain my momentum in this project. I am indebted to them.

To my Mother, Jerri Kennedy, I owe enormous gratitude. Her patience and encouragement through all of the stages of my life allowed me to become the person I am today.

TABLE OF CONTENTS

Page

Page

Page

LIST OF TABLES

Page

LIST OF FIGURES

Page

CHAPTER 1

INTRODUCTION

The morphology, chemistry, and mineralogy of modern soils result from interactions between the five primary soil forming factors: climate, organisms, relief, parent material, and time (Jenny, 1961). Although modern soil taxonomy is non-genetic, soil classification schemes generally relate soil properties to modern environmental processes and conditions, such as climate and duration of pedogenesis (Soil Survey Staff, 2010). Using modern soils as a baseline, the physical, chemical, and mineralogical properties of paleosols, such as relative abundance of major elements and clay minerals, and the size and position of soil horizons, have been used to reconstruct paleoclimates (Retallack, 1992, 2005, 2007; Terry, 2001; Sheldon et al., 2002; Sheldon and Retallack, 2004; Sheldon and Tabor, 2009), along with other proxies including stable isotopes (Sheldon and Tabor, 2009), leaf morphology (Wolfe, 1978; Uhl et al., 2007), and comparative paleophysiology (Leopold and Clay-Poole, 2001; Utescher and Mosbrugger, 2007). Geochemical proxies are often used as a quantitative measure of pedogenic products and thus processes (Retallack, 1992, 2005, 2007; Terry, 2001; Sheldon et al., 2002; Retallack et al., 2004; Sheldon and Retallack, 2004; Sheldon and Tabor, 2009). Modern soil chemical data published by Marbut (1935) have been developed into a series of climofunctions which quantitatively relate the chemical composition of modern soils to mean annual precipitation (MAP) and mean annual temperature (MAT) (Nesbitt and Young, 1982; Maynard, 1992; Retallack, 1992, 2005; Sheldon et al., 2002; Nordt et al., 2006; Sheldon and Tabor, 2009).

In modern environments where climate and lithology are constant, soil properties vary as a function of relief and drainage (Birkeland, 1999). High stability and better drainage in upland positions promote greater chemical weathering and less erosion resulting in thick, mature soils, whereas steeper slopes can truncate the active pedogenic surface producing thin, immature soils with only incipient chemical weathering (Gerrard, 1992). Variations in relief and drainage can also lead to biological partitioning which may exaggerate the differences in apparent pedogenesis along a slope (Gregory et al., 1991). The realization that slope position and drainage produce differences among contemporaneous soils along a hillslope is known as the catena concept (Milne, 1935). Although relief and drainage have been taken into account in the interpretation of modern weathering and soil-forming environments (e.g., Birkeland, 1999; Conacher and Dalrymple, 1977; Gerrard, 1992; Milne, 1935), relief has been largely ignored in paleoclimate reconstructions from paleosols (Prochnow et al., 2005). Paleoclimate reconstructions using paleosol properties and climofunctions may therefore be misleading if local paleotopography significantly affected paleosol development.

The siliciclastic and volcaniclastic strata of the White River Group record the effects of the Eocene-Oligocene Transition (EOT), a change in Earth's climate from hothouse to icehouse conditions that is marked by a major shift in the evolution of terrestrial ecosystems in North America (Miller et al., 1987; Prothero and Heaton, 1996). In this study, I investigated paleosols associated with an Early Oligocene paleovalley within the Orella Member of the Brule Formation in Toadstool Geologic Park in northwestern Nebraska. I hypothesize that topographically controlled variations in physical, chemical, and biological properties of contemporaneous paleosols located at

different physiographic positions along a paleovalley will lead to significantly different paleoenvironmental interpretations.

Paleosol macromorphology, micromorphology, bulk rock geochemistry, clay mineralogy, and pedogenic maturity were compared on the summit, shoulder, and backslope of an incised paleovalley in Toadstool Geologic Park, northwest Nebraska (Figure 1). Each paleosol was classified and climofunctions were calculated to investigate the effect of local paleorelief on the development of contemporaneous paleosols and associated paleoclimate proxies.

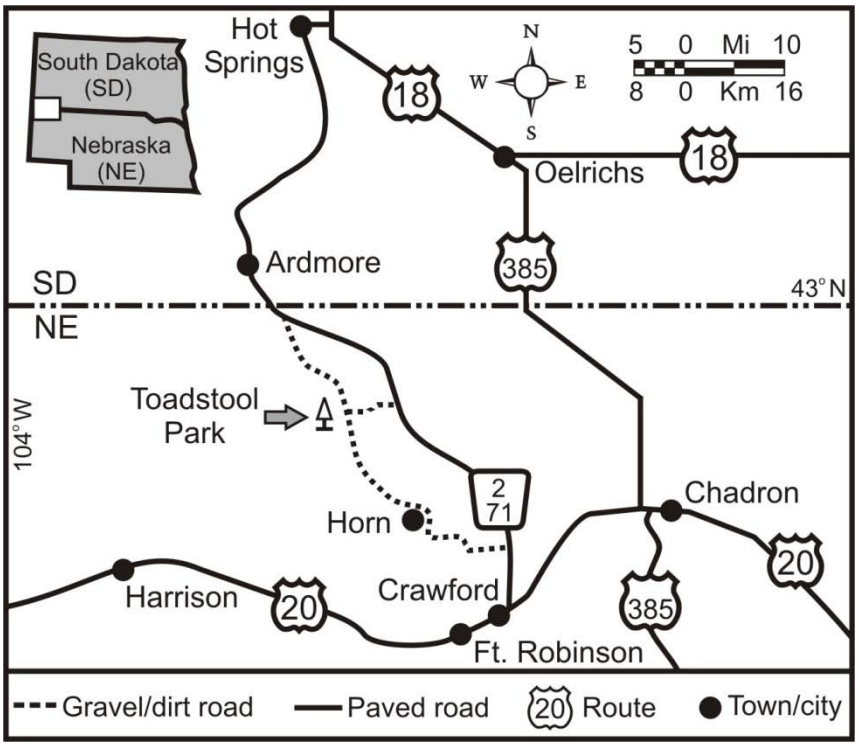

Figure 1. Location of Toadstool Geologic Park. Modified from Terry (2001).

1.1 Soil Catena Concept

Jenny (1961) suggested that soil properties and maturity depend on the interactions between climate, organisms, relief, parent material, and time. A situation can

be conceptualized in which all but one of these factors is held relatively constant, thus allowing the influence of that one factor to fully express itself. A topographic transect, revealing soils along a two dimensional slope, illustrates the influence of relief. This sequence of soils, with all else but relief in common, is called a toposequence. Slope geomorphology tends to affect pedogenesis in a systematic and predictable way. The catena concept suggests slope position and drainage primarily drive the differences among contemporaneous soils along a hillslope (Gerrard, 1992). A catena is a complex of soils along a hillslope which have certain features at idealized geomorphic positions. From most distal to most proximal to the channel these positions include: summit, shoulder, backslope, footslope, and toeslope (Figure 2).

The five positions are defined by their relative convexity/concavity. Differential pedogenesis, driven by soil erosion and hydrology, tends to segregate solutes and byproducts of hydrolysis into separate physiographic positions, thereby generating laterally contemporaneous soils with very different physical and chemical properties (Birkeland, 1999). The relative erosion potential, as well as subsurface hydrology, drive the physical and chemical differentiation of geomorphic positions. Eroded material from unstable shoulder and backslope positions are deposited in the footslope and toeslope positions whereas the relatively stable summit undergoes greater pedogenesis than the other positions. The throughflow of water removes solutes from the upland positions and tends to enrich the lowland positions.

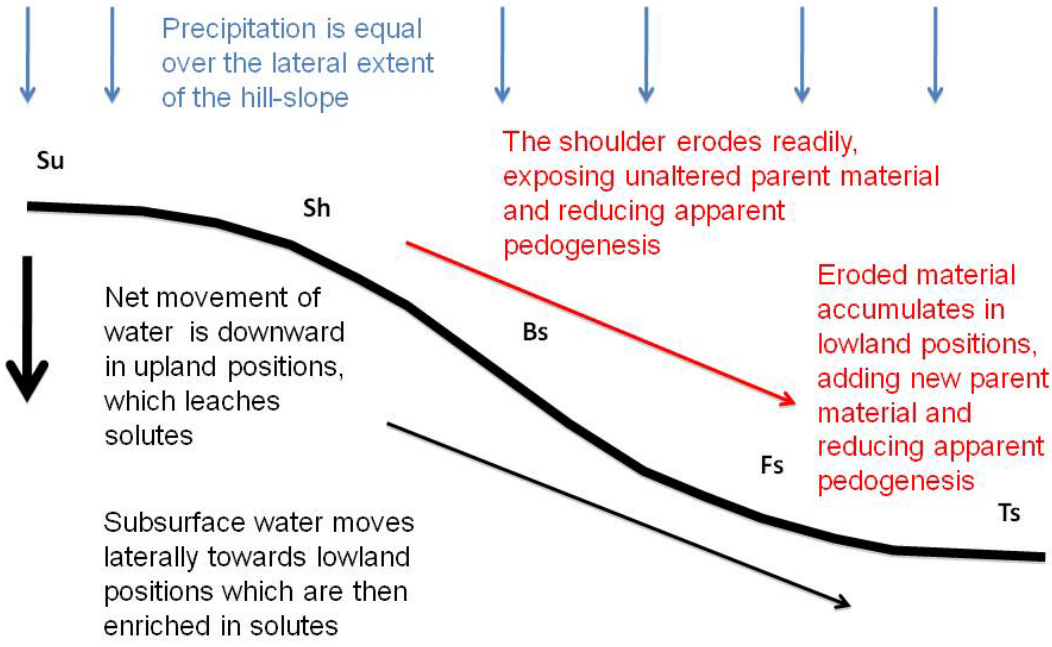

Figure 2. Idealized hillslope geomorphology and associated processes. Physiographic positions are as follows; (Su) summit, (Sh) shoulder, (Bs) backslope, (Fs) footslope, (Ts) toeslope. Modified from Birkeland (1999).

1.2 Field Area

Toadstool Geologic Park, which lies within the Oglala National Grassland, is administered by the United States Forest Service and is located about 24 km (15 miles) northwest of Crawford, NE (Figure 1). Strata exposed in Toadstool Geologic Park include the Late Eocene to Early Oligocene White River Group (Terry, 2001), which is composed largely of volcaniclastic material generated by Great Basin explosive volcanism that was subsequently redistributed via fluvial and aeolian processes, siliciclastic material from degradation of various Laramide uplifts, and occasional layers of air-fall volcanic ash (tuff) (LaGarry, 1998; Larson and Evanoff, 1998) (Figure 3).

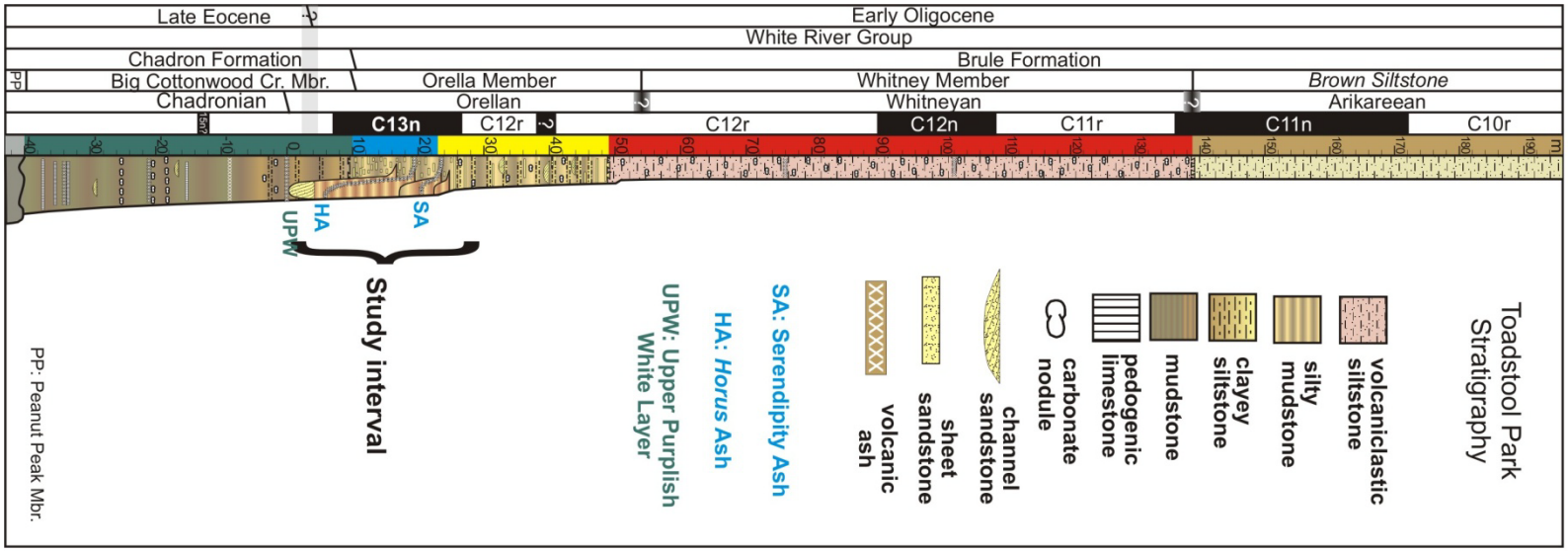

Figure 3. Stratigraphy of Toadstool Geologic Park. Modified from Grandstaff and Terry (2009).

Toadstool Geologic Park is widely studied because of its value in regional correlation of White River Group stratigraphy and paleoenvironmental reconstructions across the EOT (Schultz and Stout, 1955; Evanoff et al., 1992; LaGarry, 1998; Larson and Evanoff, 1998; Terry, 1998; Terry and LaGarry, 1998; Terry, 2001; Sheldon et al., 2002; Zanazzi et al., 2007, 2009; Grandstaff and Terry, 2009).

In Northwest Nebraska, the White River Group (comprising the Chamberlain Pass, Chadron, and Brule Formations) unconformably overlies the Upper Cretaceous Pierre Shale (Terry, 1998). The Late Eocene Chamberlain Pass Formation represents the first fluvial sediments deposited atop the Yellow Mounds Paleosol, a geosol representing intense regional pedogenic alteration of the Pierre Shale (Terry and Evans, 1994). The Late Eocene Chadron Formation, including the Peanut Peak and Big Cottonwood Creek Members, is composed of smectitic, volcaniclastic claystones with occasional thick tuff layers that are used as regional marker beds (Terry and LaGarry, 1998; Terry, 1998, 2001). These sediments are less pedogenically modified than those of the Chamberlain Pass Formation, but more modified than those of the overlying Oligocene Brule Formation and represent a change in sedimentation rate, volcanism, and/or climate, resulting in decreasing intensity of pedogenesis up-section (Terry, 2001).

The Orella Member of the Brule Formation contains fluvial siltstones and claystones interbedded between sheet sandstones and infrequent volcanic ash (LaGarry, 1998). The base of the Orella Member is composed of a series of nested paleovalleys which are incised down to the Upper Purplish White Layer within the Chadron Formation and later backfilled to form the Toadstool Park paleovalley complex (LaGarry, 1998; Terry and LaGarry, 1998). My study interval is located within the Toadstool Park

channel complex, along the exposed paleotopographic transect of a single paleovalley (Figures 3 and 4). A newly discovered volcanic ash, herein designated as the Horus Ash, caps this paleo-valley surface. It is expressed in outcrop as a dark grey band approximately 10 cm thick. In the upland area of the paleotopography it is overlain by a bright red layer which is truncated to the North by the backslope of the paleovalley. The Horus Ash extends as a marker bed into the valley fill sediments of the lowland (Figure 4). The Serendipity Ash also defines a paleosurface and overlies the Horus Ash by ~1.5 – 7 m, depending on paleotopographic position (Figure 4). Both the Serendipity Ash and the Horus Ash are currently being radiometrically dated by Sahy et al. (2010). The Orella Member is conformably overlain by the Whitney Member (Figure 3). The contact between the Orella and Whitney Members marks a transition from predominantly fluvial to predominantly aeolian facies (LaGarry, 1998). This trend of increasing aeolian influence continues into the uppermost member of the White River Group, the Brown Siltstone Member (LaGarry, 1998).

The up-section decrease in pedogenesis is attributed to a decrease in weathering as a result of cooling and aridification during and after the EOT between ~ 34.4 and ~33.6 Ma (Hilgen and Kuiper, 2009). This transition encompasses the Chadronian-Orellan North American Land Mammal Age boundary at 33.9 Ma (Prothero and Whittlesey, 1998). The opening of the Drake Passage decreased the input of warm, equatorial waters and cooled the Antarctic Ocean, facilitating the appearance of permanent polar ice caps which remain to the present (Kennett, 1977; Lagabrielle et al., 2009).

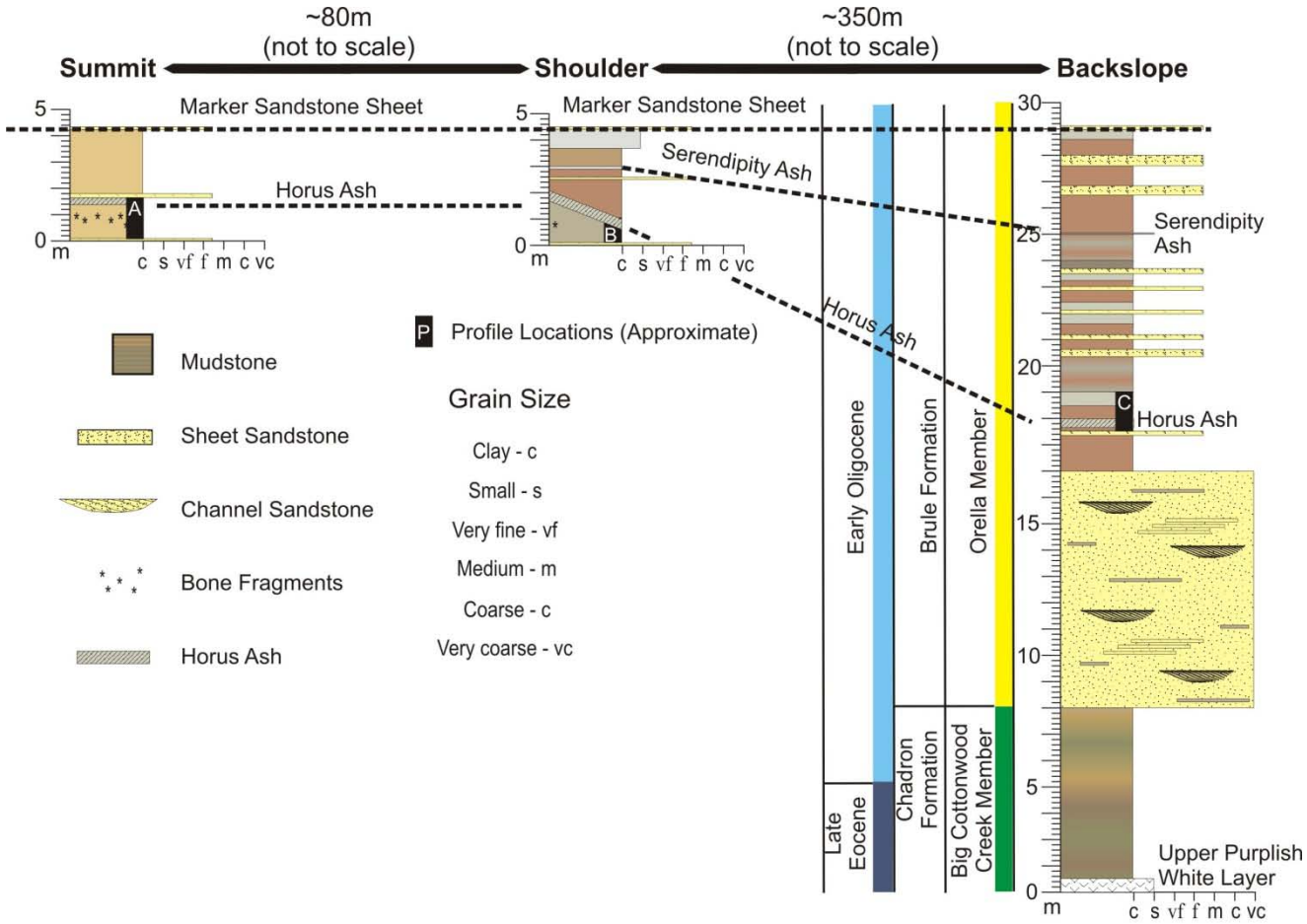

Figure 4. Measured section of the study interval. Dashed lines indicate marker beds used to correlate paleotopography. Approximate locations of profiles are indicated by black bars; (A) summit profile, (B) shoulder profile, (C) backslope profile. Note: Serendipity Ash pinches out with paleovalley fill and does not overlie the summit position. Outside of the paleovalley, the two ashes are separated by 1.5 m of strata.

The transition from the greenhouse conditions of the Late Eocene to the icehouse conditions of the Early Oligocene are marked by faunal turnovers in both marine and terrestrial environments (Evanoff et al., 1992; Billups, 2008; Aubry and Bord, 2009). Although marine isotopic records indicate global cooling of 3 – 4°C across the EOT (Zachos et al., 2001), terrestrial isotopic studies suggest MAT decreased by 7.1 ± 3.1°C at Toadstool Park (Zanazzi et al., 2007, 2009). Studies of paleosols in South Dakota using geochemical proxies of climate driven processes (climofunctions) indicate a general trend of terrestrial aridification (Retallack, 1992; Sheldon et al., 2002; Sheldon and Retallack, 2004); however, the record is complex and regionally variable (Terry and Evans, 1994; Terry, 2001; Sheldon, 2009). Environments change from fluvial to aeolian across the EOT and up section in the White River Group (Evanoff et al., 1992; LaGarry, 1998) in association with increased sedimentation rates (Grandstaff and Terry, 2009; Zanazzi et al., 2009; Griffis and Terry, 2010).

1.3 Previous Studies of Paleosols in the White River Group

Studies of paleosols in the White River Group have been mainly concerned with their potential for determination of paleoclimatic change. Retallack (1983) compared paleosol maturity through time in Badlands National Park, South Dakota. The general trend of paleosol maturity decreasing up-section was thought to represent the influence of progressive aridification. Terry and Evans (1994) also suggested that the paleosols in Badlands National Park may indicate aridification through time and also noted that paleosols along a catena record these changes differently. Terry (2001) made a more in-depth study of the paleosols of the White River Group in Northwest Nebraska and

suggested that the shift in climate during the Eocene/Oligocene may be regionally variable. McCoy (2002) investigated lateral changes in paleosol morphology across the asymmetrical basin which collected the White River Group sediments of Badlands National Park and found that paleosols could be used to infer relative paleocatenary position. Sheldon et al. (2002) and Sheldon and Retallack (2004) applied climofunctions to the Eocene/Oligocene paleosols of Oregon, Montana, and Nebraska and compared them to paleoclimate measurements inferred from the isotopes of benthic foraminifera. The correlations found in these papers are the basis of the widely used climofunctions used in this study. Metzger et al. (2004) investigated the effect of pedogenesis on the rare earth element signatures of fossil bones in Badlands National Park and found a correlation between the ratio of heavy to light rare earth elements in bone and the degree of associated pedogenesis. Stinchcomb (2007) traced a geosol along the Scenic/Poleslide Member contact in Badlands National Park and found dynamic interactions between lateral changes in sedimentation and associated pedogenesis. Sheldon (2009) and Sheldon et al. (2009) re-examined paleosols as a record of terrestrial climate in White River Group and globally comparable strata in North America and Europe and suggest, that local variation in paleoclimatic influences on pedogenesis are due to orogenic effects and differences in global climate patterns. Griffis and Terry (2010) compared paleosol development through time in White River Group material at Flagstaff Rim near Casper, Wyoming and suggested that the decrease in apparent pedogenesis up-section is due to an increase in sedimentation rate, as well as a drop in mean annual precipitation.

CHAPTER 2

MATERIALS AND METHODS

2.1 Field Work and Macromorphology

The study interval at Toadstool Geologic Park is a two-dimensional transect of a paleovalley approximately 400 m long and 0 – 10 m deep (Figure 4). Three distinct paleogeomorphic zones are evident based upon their relative slope and geomorphological associations (Figure 4). A marker sandstone sheet was used to visually aid the recognition of paleotopography and the determination of slope (Figure 4). The flat-lying summit area has a measured paleo-slope of ~2%. The steeply graded shoulder area has a measured paleo-slope of ~10%. The more gently graded backslope area has a paleo-slope of ~5%. Footslope and toeslope positions are missing due to modern erosion. Outcrops in the White River Group have been compacted to ~70% of the original thickness of material according to Terry (2001), thus paleo-slope measurements be slightly lower than original values.

Three paleosol profiles were sampled by digging vertical trenches to expose fresh material. All three trenches were dug at distinct paleo-geomorphic positions as determined by change of paleo-slope. The profiles included material between bounding sheet sands which bracketed the Horus Ash in order to ensure isochrony among paleosol profiles (Figure 4). Bulk samples were collected every 10 cm. Oriented samples were collected from select paleosol horizons chosen for their diagnostic soil characteristics. Paleosol features identified and recorded in the field included: Munsell® soil color

(fresh) (Munsell Color, 2000), root traces, rip-up clasts, slickensides, soil structure, mottling, relict sedimentary structures, and grain size.

2.2 Soil Micromorphology

Oriented samples were dry cut and polished to a thickness of 30 μm on a dry lap wheel to minimize the expansion of abundant smectite in the samples and then mounted on petrographic slides using low viscosity, two component epoxy resin. Samples prone to disaggregation were first vacuum impregnated with epoxy before dry cutting. Soil plasmic fabric, root traces, relative grain size, and secondary mineralization were examined using a Nikon E600 polarizing microscope. Photomicrographs were taken using a Nikon DXM 1200F digital camera. Soil plasmic fabrics were classified according to Nahon (1991).

2.3 Clay Mineralogy

The clay size fraction of the surface samples of each profile was separated via gravitational settling and Millipore filtration (Moore and Reynolds, 1997). Oriented samples were transferred to petrographic slides and scanned on a Rigaku D-Max B x-ray diffractometer at Temple University from 2° to 30° 2θ with a 1.2°/minute step using CuKα radiation at 15mA and 30 KV. X-ray spectra of samples treated with ethylene glycol were compared with those of air-dried samples to aid the determination of clay mineral composition.

2.4 Bulk Rock Geochemistry and Molecular Weathering Ratios

Forty six bulk samples were analyzed for whole-rock chemical composition. The samples were powdered to ~150 μm using a mullite-chamber shatterbox. The powdered samples were sent to Franklin and Marshall College for X-Ray fluorescence analysis. Major element samples were prepared by fusing a glass disk made of 0.4000 ± 0.0001 g whole rock powder and 3.6000 ± 0.0002 g lithium tetraborate in a Pt crucible (Franklin and Marshall, 2010). Trace element samples were pressed into a pellet of 7.0000 ± 0.0004 g whole rock powder and 1.4000 ± 0.0002 g copolywax powder (Franklin and Marshall, 2010). Major element samples and trace element samples were analyzed using a Phillips 2404 XRF vacuum spectrometer (Franklin and Marshall, 2010). Geochemical data were converted into moles by dividing the data (ppm or weight percent of oxide) by the molecular mass of the element or oxide before being used to calculate molecular weathering ratios (Sheldon and Tabor, 2009).

Molecular weathering ratios relate pedogenic processes to their resulting products by comparing the relative abundance of elements (Sheldon and Tabor, 2009). Numerous molecular weathering ratios are used to infer relative intensity of weathering, or associate weathering with select processes and products (Table 1). The molecular weathering ratio $\frac{CaO+MgO+Na_2O+K_2O}{Al_2O_3}$ or $\frac{\sum BASES}{Al_2O_3}$ is used as an analogue of soil base saturation (Sheldon et al., 2002). A $\frac{\sum BASES}{Al_2O_3}$ value of 0.5 is considered to represent 35% base saturation (Sheldon, et al., 2002). This makes paleosols with $\frac{\sum BASES}{Al_2O_3} > 0.5$ Alfisol-like, and those with $\frac{\sum BASES}{Al_2O_3} < 0.5$ Ultisol-like (Sheldon et al., 2002). Another widely used molecular weathering ratio, the Chemical Index of Weathering $(CIW) = 100 \times (\frac{Al_2O_3}{Al_2O_3+CaO+Na_2O})$,

accounts for potential diagenetic redistribution of K (Sheldon and Tabor, 2009). The CIW, which is sometimes referred to as the Chemical Index of Alteration Minus Potassium (CIA-K), was independently developed by Harnois (1988) and Maynard (1992) to account for separate redistributions of K in soils (Sheldon and Tabor, 2009). The ratio $\frac{Al_2O_3}{SiO_2}$ (clayeyness) infers hydrolysis from production of authigenic clay minerals, as well as sedimentary changes in grain size, assuming uniform parent mateiral (Sheldon and Tabor, 2009).

Table 1. Climofunctions used in this study

Climofunction	Molecular Weathering Ratio	Justification	Empirical Fit
$T(°C\ MAT) = -18.5S + 17.3$	Salinization (S) $= \frac{K_2O + Na_2O}{Al_2O_3}$	Accumulation of evaporated salts: occurs in hot, arid climates.	$R^2 = 0.37$
$T(°C\ MAT) = 46.9C + 4$	$(C) = \frac{CaO}{Al_2O_3}$	Solutes accumulate relative to clay minerals during hydrolysis.	$R^2 = 0.96$
$P(mm\ yr^{-1}\ MAP) = 253.9Ln\left(\frac{\sum BASES}{Al_2O_3}\right) + 759$	$\frac{\sum BASES}{Al_2O_3} = \frac{CaO + MgO + Na_2O + K_2O}{Al_2O_3}$	Bases are lost from primary and clay minerals during leaching.	$R^2 = 0.66$
$P(mm\ yr^{-1}\ MAP) = 221.1e^{0.0197(CIW)}$	$CIW = 100(\frac{Al_2O_3}{Al_2O_3 + CaO + Na_2O})$	Clay minerals accumulate relative to mobile elements during weathering.	$R^2 = 0.72$

After Sheldon and Tabor (2009)

The ratio represents the relative amount of clay to other mineral components because Al accumulates in clay minerals relative to the Si of silicate rocks (Sheldon and Tabor, 2009). However, this does not necessarily measure authigenic clay formation due to pedogenesis, as aeolian additions of fine grained material can skew the resulting ratio (Sheldon and Tabor, 2009). The ratios of immobile elements to one another are also thought to indicate changes in parent material or lithologic discontinuities, because relatively immobile elements should remain immobile during pedogenesis, so their ratios should remain fixed (Sheldon, 2006). Relative solubility in common soil solution chemical conditions can be an indication of leaching intensity (Sheldon and Tabor, 2009). The ratio $\frac{\mathrm{Ba}}{\mathrm{Sr}}$ is widely employed as a proxy for leaching intensity as the solubility of Sr is greater than that of Ba, although the effect of pedogenesis on Ba is not completely understood (Sheldon and Tabor, 2009). The accumulation of mobile elements within a soil (salinization) can be indicated by the ratio $\frac{\mathrm{K_2O+Na_2O}}{\mathrm{Al_2O_3}}$ (Sheldon and Tabor, 2009). Trace elements such as Cu and Ni can form complexes with soil organic material and illuviated colloids, and their net abundance can be used as an indication of the separate zones of eluviation and illuviation in soils and paleosols (Terry, 2001; Kahnmann et al., 2008). Phosphorus is also associated with the organic component of soils, and may indicate paleofertility when compared to the abundance of immobile elements such as in the ratio $\frac{\mathrm{P_2O_5}}{\mathrm{TiO_2}}$ (Sheldon and Tabor, 2009).

2.5 Calculation of Paleoclimate Proxies

Paleoclimate proxies utilize the bulk composition data from the zone of illuviation (B horizon) of the subsoil in an equation which is calibrated from measurements of modern soil compositions in varied climates (Sheldon and Tabor, 2009). Base saturation is also used as a proxy for paleoprecipitation, as bases are leached by hydrolysis from primary and Al-bearing clay minerals (Sheldon and Tabor, 2009) (Table 1). The paleoprecipitation climofunction associated with CIW infers the same process of base loss as in the $\frac{\sum \text{BASES}}{Al_2O_3}$ approach, and the two climofunctions often show an inverse relationship because of the presence of Al_2O_3 in the numerator of CIW and the denominator of $\frac{\sum \text{BASES}}{Al_2O_3}$ (Sheldon and Tabor, 2009) (Table 1). While $\frac{\sum \text{BASES}}{Al_2O_3}$ is more widely applicable among different parent materials, CIW is better suited to deal with paleosols because it does not use the abundance of K which can be added during diagenesis (Sheldon and Tabor, 2009).

Paleotemperature can also be calculated by comparison of the geochemical proxy of molecular weathering ratios to modern soil climate measurements (Sheldon and Tabor, 2009). For example, the evaporative conditions of deserts are associated with high temperatures (Sheldon and Tabor, 2009). Measurements of the salinization ratio $\frac{K_2O+Na_2O}{Al_2O_3}$ are compared to MAT to build an equation to predict paleothermometry (Sheldon and Tabor, 2009). Hydrolysis is driven by temperature as well as precipitation, thus the ratio of $\frac{Al_2O_3}{SiO_2}$ is used in an equation derived from modern measurements of temperature (Sheldon and Tabor, 2009).

CHAPTER 3

RESULTS

3.1 Macromorphology

3.1.1 Summit

Two zones of fining upward grain size are present in the summit profile, with a boundary between the two at ~100 cm depth (Figure 5). Hairline, drab-haloed root traces were found throughout the summit profile (Table 2). Incipient, blocky soil structure was found in the upper 10 cm of the profile and from ~70 cm depth down to the bottom of the profile (Table 2; Figure 5). The upper 10 cm of the profile was noticeably darker (10YR 6/2) than the rest of the profile (10YR 7/2) and also contained small (1-2 mm diameter) rip-up clasts (Table 2; Figure 5). This upper 10 cm of the profile is the Horus Ashfall layer, which marks the paleosurface of the paleocatena in the study area (Table 2; Figures 3 and 4). Above the Horus Ashfall is a very thin (1-2 cm) layer of reddish, massive claystone (Figure 6a).

Table 2. Description of Summit Profile

Depth	Horizonation	Macroscopic features	Microscopic features
0 - 10 cm	A	Light brownish grey (10YR 6/2) matrix, pale green (7/5G) drab-haloed root traces (hairline), incipient soil structure, few rip-up clasts (1-2 mm diameter).	Quartz grains and slightly weathered volcanic glass shards, few mica and hematite grains, secondary zeolites, small calcium carbonate rhizoliths (~10-50 μm), lattisepic fabric.
10 - 20 cm	AB	Light grey (10YR 7/2) matrix, pale green (7/5G) drab-haloed root traces (hairline).	NA

Table 2. (continued)

Depth	Horizonation	Macroscopic features	Microscopic features
20 - 60 cm	Btk	Light grey (10YR 7/2) matrix, pale green (7/5G) drab-haloed root traces (hairline).	Quartz grains and slightly weathered volcanic glass shards, few mica and hematite grains, Stage I – II pedogenic carbonate glaebules, few argilans, secondary zeolites, small calcium carbonate rhizoliths (~10-50 µm), lattisepic fabric.
60 - 100 cm	Bw	Light grey (10YR 7/2) matrix, pale green (7/5G) drab-haloed root traces (hairline), incipient soil structure, bone fragments (1-2 mm).	Quartz grains and slightly weathered volcanic glass shards, few mica and hematite grains, secondary zeolites, small calcium carbonate rhizoliths (~10-50 µm), lattisepic fabric.
100 - 180 cm	2AB	Light grey (10YR 7/2) matrix, pale green (7/5G) drab-haloed root traces (hairline), incipient soil structure.	Quartz grains and slightly weathered volcanic glass shards, few mica and hematite grains, secondary zeolites, small calcium carbonate rhizoliths (~10-50 µm), lattisepic fabric.
180 – 210 cm	2BC	Light grey (10YR 7/2) matrix, pale green (7/5G) drab-haloed root traces (hairline), incipient soil structure.	Quartz grains and slightly weathered volcanic glass shards, few mica and hematite grains, secondary zeolites, small calcium carbonate rhizoliths (~10-50 µm), lattisepic fabric.

'NA' indicates missing oriented sample material due to in-field horizon designations which were later found to be spurious.

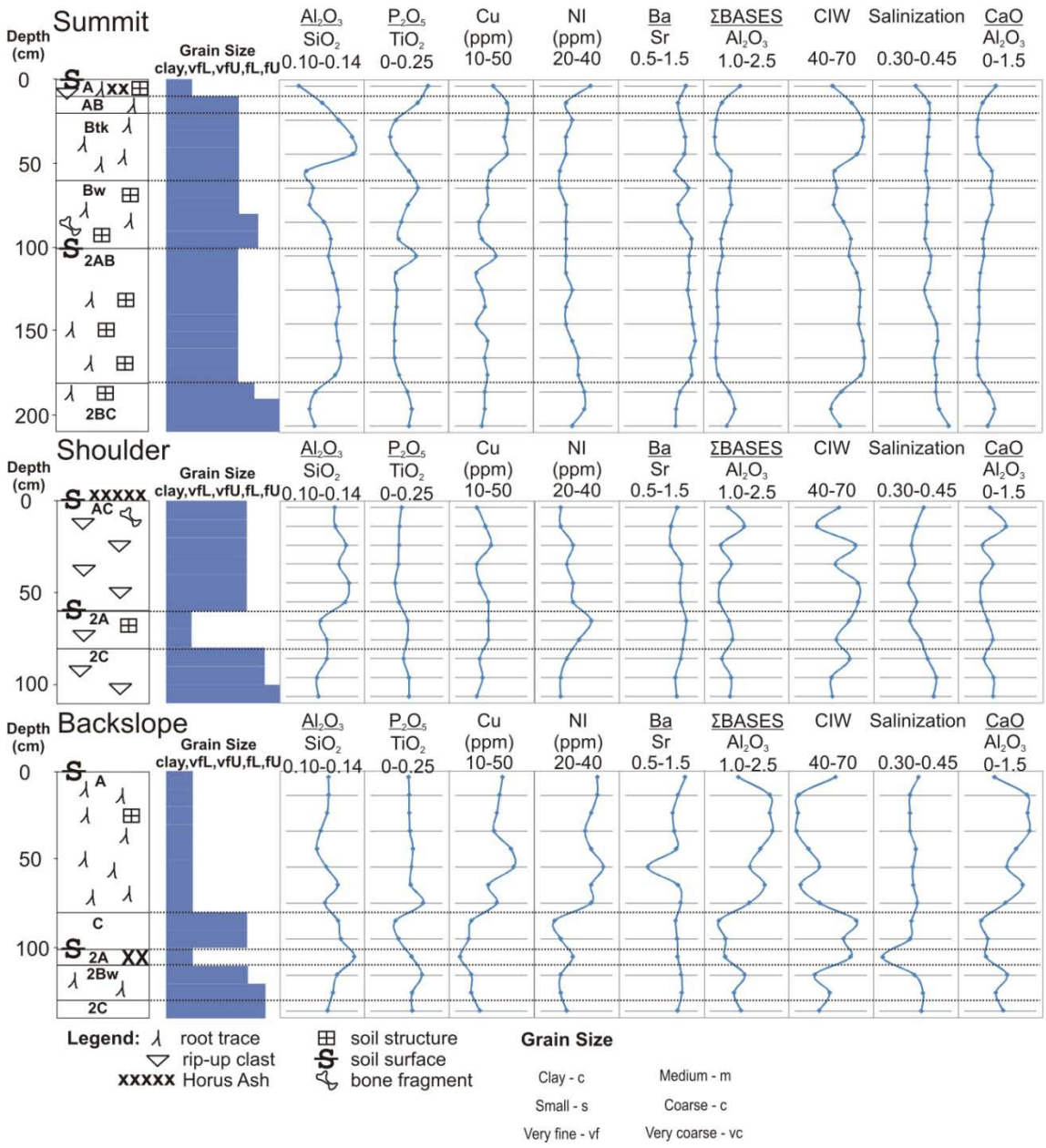

Figure 5. Paleosol morphology and molecular weathering ratios of profiles along the paleotopography of figure 4.

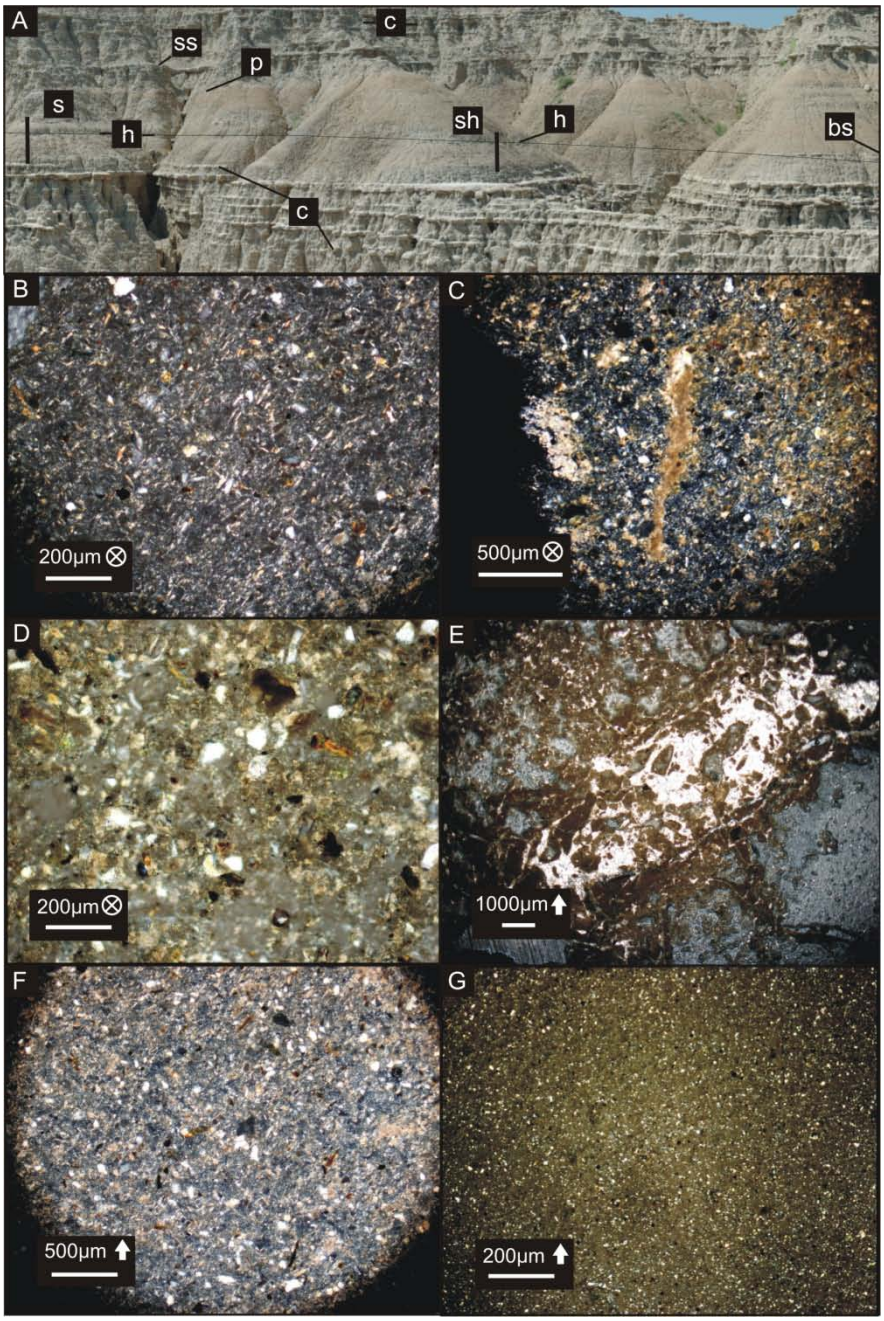

Figure 6. Field photo-stitch of the study interval and photomicrographs of selected paleosol features; (A) paleovalley exposure; (h) Horus dark layer, (ss) marker sheet sand, (p) paleovalley fill pinching out, (c) crevasse splay sands, and positions of (s) summit and (sh) shoulder trenches. The backslope trench (bs) is out of the photograph to the right, (B) Summit Paleosol lattisepic fabric, (C) Summit Paleosol rhizolith and pedogenic carbonate glaebules, (D) Shoulder Paleosol matrix, (E) Backslope Paleosol rhizolith, (F) lower Backslope Paleosol lattisepic fabric, (G) upper Backslope Paleosol isotic fabric. Arrows indicate up direction in photomicrographs, whereas crosshairs indicate photomicrographs in plan-view.

3.1.2 Shoulder

Grain size in the shoulder profile becomes finer from the bottom of the profile up to ~60 cm depth, where it becomes coarse and remains the same up to the top of the profile (Figure 5). Rip-up clasts (1-2 mm diameter) are present throughout the profile, which increase in size (1-5 mm diameter) with depth (Table 3; Figure 5). Incipient soil structure is present from ~60 cm depth to ~80 cm depth, within the finest sediments of the profile (Table 3; Figure 5). The Horus Ashfall lies just above the top of the profile, making the top of the shoulder profile contemporaneous with the top of the summit profile (Figures 4 and 5).

Table 3. Description of Shoulder Profile

Depth	Horizonation	Macroscopic features	Microscopic features
0 - 60 cm	AC	Light grey (10YR 7/2) matrix, rip-up clasts (1-2 mm diameter).	Quartz grains and slightly weathered volcanic glass shards, few mica and hematite grains, secondary zeolites, cancellous bone fragments, isotic fabric.
60 - 80 cm	2A	Light brownish grey (10YR 6/2) matrix, incipient soil structure, rip-up clasts (1-5 mm diameter).	Quartz grains and slightly weathered volcanic glass shards, few mica and hematite grains, secondary zeolites, isotic fabric.
80 - 110 cm	2C	Light grey (10YR 7/2) matrix, rip-up clasts (1-5 mm diameter).	Quartz grains and slightly weathered volcanic glass shards, few mica and hematite grains, secondary zeolites, isotic fabric.

3.1.3 Backslope

Two zones of fining upward grain size are preserved in the backslope profile, with a boundary between the two at ~100 cm depth (Figure 5). The upper 80 cm of the profile was very fine grained. The upper 20 cm of the profile contained moderate (1-5 mm diameter) clay-filled root traces, and from ~20 cm depth to ~80 cm depth there were large (~5 mm diameter) drab-haloed root traces (Table 4; Figure 5). The Horus Ashfall is preserved within the backslope profile at ~110 cm depth as a thin (~1 cm) layer of fine volcanic ash (Table 4; Figure 5).

Table 4. Description of Backslope Profile

Depth	Horizonation	Macroscopic features	Microscopic features
0 - 80 cm	A	Light brownish grey (10YR 6/2) to brown (10YR 5/3) matrix, clay filled root traces (1-5 mm diameter), pale green (7/5G) drab-haloed root traces (~5 mm diameter), incipient soil structure.	Secondary calcite and zeolites, large (~1 mm diameter) calcium carbonate rhizoliths, sediment too fine for further grain identification.
80 - 100 cm	C	Light brownish grey (10YR 6/2) matrix.	NA
100 – 110 cm	2A	Brown (10YR 5/3) matrix, Horus Ash.	NA
110 - 130 cm	2Bw	Greyish brown (10YR 5/2) matrix, pale green (7/5G) drab-haloed root traces (hairline).	Quartz grains and slightly weathered volcanic glass shards, few mica and hematite grains, secondary zeolites, lattisepic fabric.
130 - 140 cm	2C	Greyish brown (10YR 5/2) matrix.	NA

'NA' indicates missing oriented sample material due to in-field horizon designations which were later found to be spurious.

3.2 Micromorphology

3.2.1 Summit

Quartz grains and very slightly weathered volcanic glass shards were found throughout the profile, as well as a few grains of mica and hematite. Secondary zeolites were also present in matrix voids. A few argilans were found in the upper part of the profile, as well as glaebules of stage I to stage II pedogenic carbonate. Very strong lattisepic plasmic fabric was found throughout the profile, along with small calcium carbonate rhizoliths (Table 2; Figure 6b, c).

3.2.2 Shoulder

Quartz grains and very slightly weathered volcanic glass shards were found throughout the profile, as well as a few grains of mica and hematite. Secondary zeolites were also present in matrix voids throughout the profile. Fragments of cancellous bone were found in the upper 60 cm of the profile. Grain size was relatively large compared to the other profiles, and isotic fabric was dominant (Table 3; Figure 6d).

3.2.3 Backslope

The upper 110 cm of this profile were almost entirely clay-sized material which was difficult to differentiate, even under magnification. This lower portion contained slightly weathered quartz grains and slightly weathered volcanic glass shards, as well as a few mica and hematite grains, and secondary zeolites. The material above ~ 80 cm included secondary carbonate and secondary zeolites. This upper material also included

many large calcium carbonate rhizoliths (Figure 6e). The fabric of the coarser, lower portion was lattisepic, while that of the fine-grained upper portion was isotic (Table 4; Figure 6f, g).

3.3 Bulk Geochemistry

3.3.1 Summit

The trend of clayeyness ($\frac{Al_2O_3}{SiO_2}$) includes two major zones of concentration with depth, each followed by a sharp decrease in value (Figure 5). Low values of clayeyness generally coincide with grain size boundaries in the summit profile, although not consistently. The paleofertility index ($\frac{P_2O_5}{TiO_2}$) is high at the top of the profile and at ~ 70 cm depth, as well as at the boundary between the two fining upward sequences at ~100 cm depth, and at the bottom of the profile. The abundance of Cu generally decreases with depth in the summit profile, but is higher just below the top of the profile, from ~20 cm depth to ~50 cm depth, and at the boundary between the two fining upward sequences at ~100 cm depth. The abundance of Ni generally increases with depth, with high values at the top of the profile and near the bottom. The ratio of $\frac{Ba}{Sr}$ is relatively constant with depth. There is a slight deflection in the value of $\frac{Ba}{Sr}$ at the top of the profile and at ~70 cm depth. There is also a decrease from ~180 cm depth down to the bottom of the profile. The $\frac{\sum BASES}{Al_2O_3}$ ratio is relatively constant thoughout, with the exception of a decrease in the upper profile from ~20-40 cm depth, and an increase in the bottom 30 cm of the section.

The trend of CIW is the inverse of $\frac{\sum BASES}{Al_2O_3}$. Salinization ($\frac{K_2O+Na_2O}{Al_2O_3}$) generally increases with depth. The trend of the ratio $\frac{CaO}{Al_2O_3}$ follows that of $\frac{\sum BASES}{Al_2O_3}$.

3.3.2 Shoulder

The value of clayeyness ($\frac{Al_2O_3}{SiO_2}$) is generally greater above ~60 cm depth, where it increases with depth, below which it decreases with depth (Figure 5). This break in the trend of clayeyness coincides with a major change in grain size in the shoulder profile at ~60 cm depth. Paleofertility ($\frac{P_2O_5}{TiO_2}$) is generally greater below ~60 cm depth, and overall increases with depth in the profile. The abundance of Cu is relatively constant throughout the profle, with a deviation at ~30 cm depth and a general decrease in the bottom of the profile. The abundance of Ni increases with depth down to ~60 cm depth, below which it decreases with depth. The ratio of $\frac{Ba}{Sr}$ is generally consistent with depth to ~60 cm, but shows a deflection at ~ 30 cm and a general decrease below ~60 cm. The trend of $\frac{\sum BASES}{Al_2O_3}$ in the shoulder profile is erratic throughout. The trend of CIW is the inverse of $\frac{\sum BASES}{Al_2O_3}$, and generally increases with depth. The value of salinization ($\frac{K_2O+Na_2O}{Al_2O_3}$) shows an overall increase downward through the profile, but increases faster below ~60 cm depth. The trend of $\frac{CaO}{Al_2O_3}$ follows that of $\frac{\sum BASES}{Al_2O_3}$.

3.3.3 Backslope

The value of clayeyness ($\frac{Al_2O_3}{SiO_2}$) generally increases with depth to the Horus Ashfall at ~110 cm depth, although there are decreases at ~50 and ~80 cm depth. Below the Horus Ashfall ($\frac{Al_2O_3}{SiO_2}$) decreases with depth in the backslope profile (Figure 5). There are Paleofertility ($\frac{P_2O_5}{TiO_2}$) varies little above ~80 cm depth (Figure 5). There are highs of paleofertility at ~80 cm depth and at the Horus Ashfall at ~110 cm depth. The abundance of Cu generally decreases with depth in the profile, with noticeable highs from ~50 cm depth to ~ 60 cm depth, and at ~80 cm depth. The abundance of Cu is lowest at the Horus Ashfall at ~110 cm depth. Trends in the abundance of Ni in the backslope profile generally follow those of Cu, except at the Horus Ashfall, where Ni increases rather than decreases. The ratio of $\frac{Ba}{Sr}$ varies little in the backslope profile, with a high at the top of the profile and a sharp decline at ~60 cm depth. The value of $\frac{\sum BASES}{Al_2O_3}$ is greater above ~80 cm depth, with low points at the top of the profile and at ~60 cm depth, and a high point at the Horus Ashfall at ~110 cm depth. The trend of CIW is the inverse of $\frac{\sum BASES}{Al_2O_3}$. The value of salinization ($\frac{K_2O+Na_2O}{Al_2O_3}$) increases slightly with depth, and has a sharp decrease at the Horus Ashfall at ~110 cm depth. The trend of $\frac{CaO}{Al_2O_3}$ follows that of $\frac{\sum BASES}{Al_2O_3}$.

3.4 Clay Mineralogy

Diffractograms of glycolated surface samples from all three profiles show diagnostic peaks of smectite and illite at 5.2° 2θ and 8.8° 2θ respectively, as well as 26.6° 2θ (Figure 7). Glycolation shifts peaks and indicates mixed-layer illite/smectite. There is

also α-cristobalite and gypsum present in all three profiles, although their peaks are of varying intensity. The Summit Paleosol has less mixed layer illite/smectite than either the Shoulder or the Backslope Paleosol, as well as less gypsum. The Summit Paleosol also contains more α-cristobalite. There is no kaolinite or calcite in the clay-size fraction.

3.5 Climofunctions

The application of common climofunctions resulted in the values reported in Tables 5 and 6. Climofunctions are calculated using averaged data from the B horizon of a soil (Sheldon and Tabor, 2009). No climofunctions were calculated for the Shoulder Paleosol as it lacks a B horizon. The values for the Backslope Paleosol horizon are almost always noticeably different from both Summit Paleosol horizons. However, none of the differences in any climofunction values between physiographic positions is statistically significant (Figure 8).

Table 5. Calculated climofunctions for Summit horizons

Sample depth	P(CIA-K) (± 181 mm/year)	P(BASES/Al) (± 235 mm/year)	T(Al/Si) (± 0.6 °C)	T((K+Na)/Al) (± 4.4 °C)
Btk				
-30 cm	853	724	10.1	9.8
-40 cm	859	732	10.4	9.9
-50 cm	817	719	10.5	9.9
-60 cm	678	663	9.2	10.0
Bw				
-70 cm	690	668	9.4	9.9
-80 cm	673	662	9.3	9.9
-90 cm	729	685	9.7	9.9
-100 cm	775	702	9.9	10.0
Average	759	694	9.8	9.9

Table 6. Calculated climofunctions for Backlope horizon 2Bw

Sample depth	P(CIA-K) (± 181 mm/year)	P(BASES/Al) (± 235 mm/year)	T(Al/Si) (± 0.6 °C)	T((K+Na)/Al) (± 4.4 °C)
-110 cm	572	618	10.0	10.4
-120 cm	646	654	9.9	10.1
Average	609	636	10.0	10.2

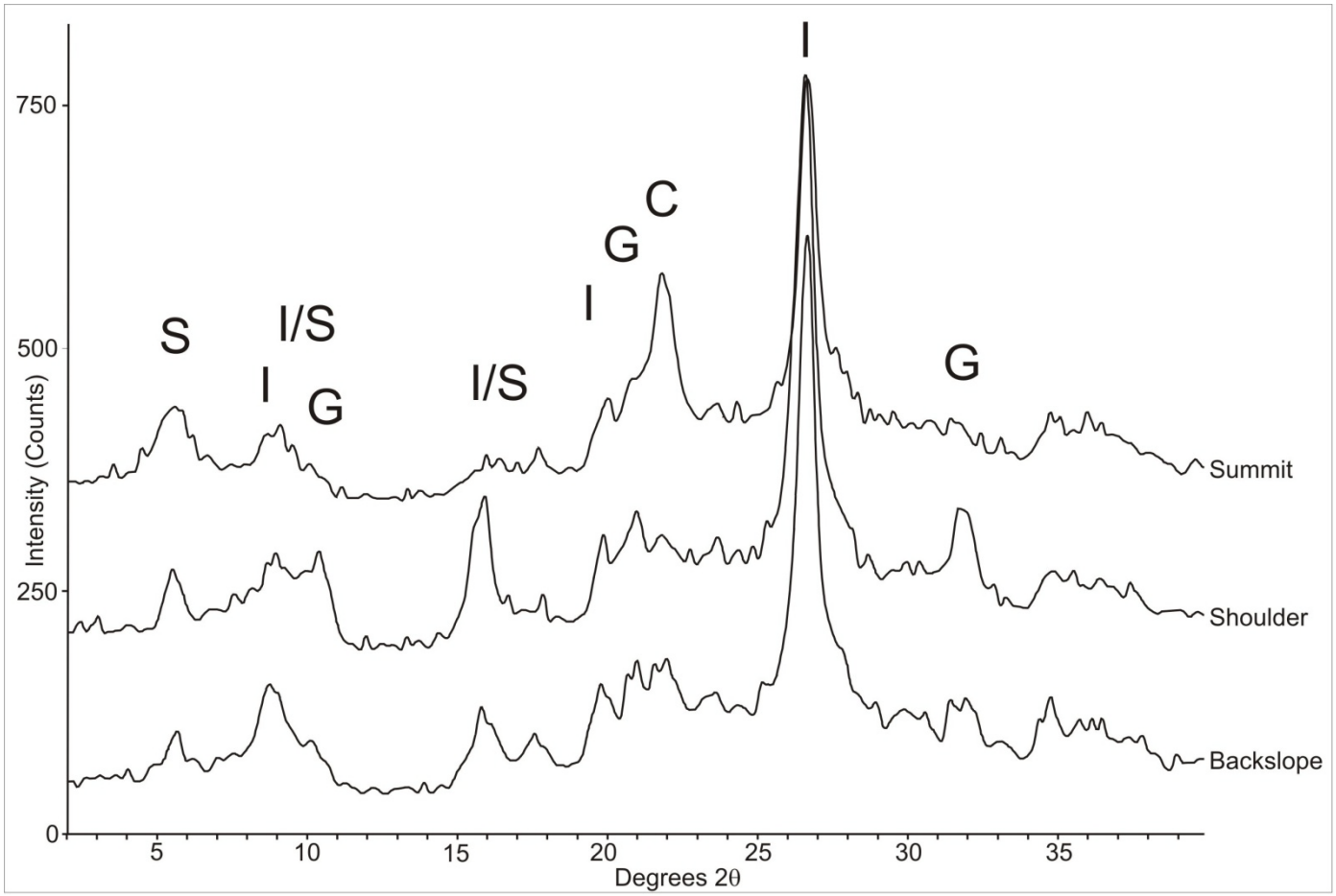

Figure 7. X-ray diffractograms of glycolated samples from the uppermost surface of each profile. (S) smectite, (I) illite, (G) gypsum, (C) α-cristobalite.

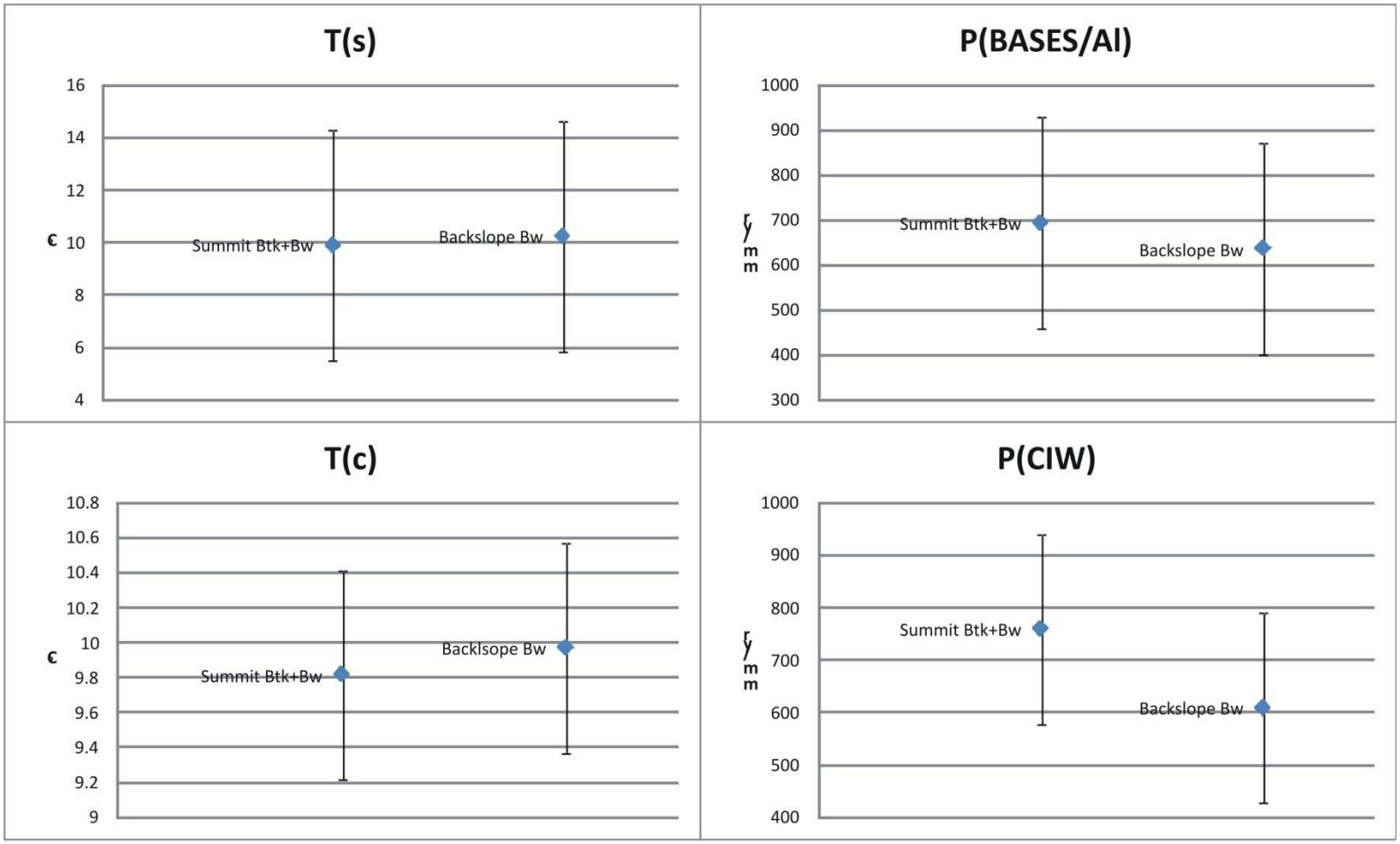

Figure 8. Average values of P(CIW), P(BASES), T(C), and T(S) of paleosols, plotted with inherent error, after Sheldon and Tabor (2009). Note the difference in scale between T(C) and T(S).

31

CHAPTER 4

DISCUSSION

4.1 Paleocatena

Across the ~400 m paleocatena observed in this study, climate would have been a uniform soil forming factor; however, the soil features used to infer climatic conditions may differ depending on relief. The soil forming factor of relief is the independent variable of this study (Jenny, 1961). Relief differs among all three soil profiles (Figure 4), and is assumed to be forcing the apparent differences in many other factors (Figure 2). The sediments of the WRG are mixed volcaniclastic and siliciclastic materials which share common source areas (Figure 3). Parent material is relatively uniform in terms of provenance and composition, with differences in grain size distribution in the summit and shoulder position due to fluvial deposition prior to paleovalley downcutting, while in the backslope position it is related to channel proximity within the active Horus paleovalley complex (Figures 4, 5a, b, and 6b, d, e). The fill material of the paleovalley was bright red at the contact with the Horus paleosurface. However, it varied in color throughout the entire backfill interval. This fill material was finer grained than the strata which were cut by the paleovalley, and was less resistant to erosion (Figures 4, 5a, b, and 9).

The temporal evolution of the paleolandscape can be conceptualized as relative durations of pedogenesis, where surface stability leads to greater soil maturity (Figure 9). The geomorphic history of this paleolandscape has allowed for various regimes of degradation, aggradation, and stability to alter sediments differently according to the soil forming factor of time (Figure 9). Pedogenically modified materials, which were

deposited and modified prior to the cutting of the Horus paleovalley, re-entered the zone of active pedogenesis as downcutting proceeded and became pedogenically welded with the development of the summit profile (T1 of Figure 9). Pedogenesis at the shoulder position was continuously truncated by erosion while the summit, and later the backslope, developed greater soil maturity (T2-T5, Figure 9). Pedogenesis at the summit and backslope, over the same amount of time, modified different amounts of parent material (Figure 9). The total time of soil development in the summit profile, which continuously modified the same package of sediment, was spread out over multiple pulses of sediment accumulation at the backslope position (Figure 9).

Root trace diameter and depth of root penetration differ along the paleocatena, as well as elemental species indicative of organic matter. Root traces are more numerous and deeper in the summit profile than in the backslope profile, and are absent from the shoulder profile. Paleofertility is greatest in the summit profile, while Cu and Ni enrichment are greatest in the backslope profile. This suggests that the activity of organisms may be partitioned along riparian boundaries, with different plant communities promoting different types and degrees of pedogenesis (Tables 2, 3, and 4; Figures 5a, b, and 6c, e). Relative pedogenic maturity also indicates that the partitioning of organisms is influencing catenary differentiation. Soil fabric is most developed, and CIW indicates the greatest weathering, in the summit profile (Tables, 2, 3, 4, and 7).

4.1.1 Summit

The two main sedimentary packages of the summit profile were deposited before the episode of downcutting that formed the paleovalley since they lie below the Horus Ash which fell on the paleovalley landscape (Figures 4 and 9). The reddish massive clay

which caps the Horus Ash at this position is backfill material which eventually overtopped the entire paleovalley (Figures 4, 6a, and 9). There are two distinct pedogenic surfaces in the Summit Profile at the top of the profile and at ~100 cm depth. These are indicated by the boundaries of sedimentary packages as well as increases in paleofertility and Cu (Figure 5). Multiple zones of leaching ($\frac{Ba}{Sr}$) and weathering (CIW) suggest multiple episodes of pedogenesis overprinting previous soils (Table 2; Figures 5 and 9). Many small root traces occur throughout the entire depth of the profile, although they represent the aggregate of multiple welded pedogenic surfaces (Table 2; Figures 5, 6c, and 9).

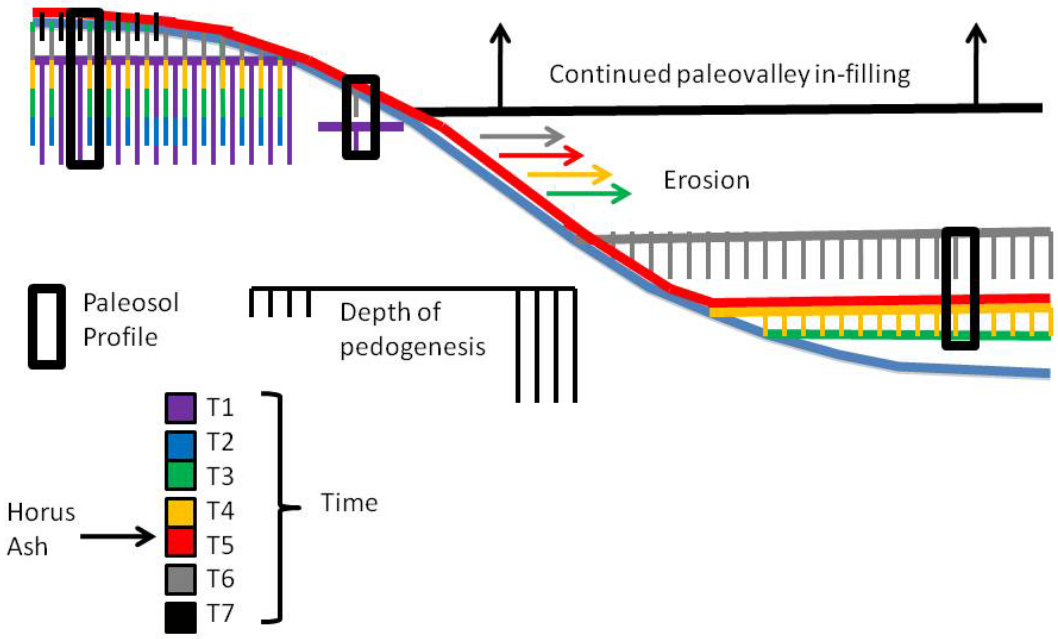

Figure 9. Idealized temporal evolution of the paleovalley. (T1) Before paleovalley incision, (T2) Paleovalley incision, (T3) Pre-Horus aggradation, (T4) Pre-Horus pedogenesis, (T5) Horus Ashfall, (T6) Post-Horus aggradation and pedogenesis, (T7) Continued paleovalley in-filling.

Clayeyness ($\frac{Al_2O_3}{SiO_2}$) responds to overall sedimentary packages, generally decreasing with coarser sediments. However, at the very top of the profile the weathering of silica-rich ash is skewing the clayeyness ratio, as suggested by the presence of the cristobalite in association with the Horus Ashfall layer (Figure 5). Paleofertility ($\frac{P_2O_5}{TiO_2}$), and Cu designate zones of organic matter accumulation in this profile. Organic matter first accumulates at the stable surface as plant detritus, after which it can be incorporated into subsurface sediments via translocation. High ($\frac{P_2O_5}{TiO_2}$) ratios at the top of the profile and at ~100 cm indicate relatively stable pedogenic surfaces. Soil structure appears at ~60 cm depth, indicating a change in horizonation, and bone fragments were found at ~100 cm, suggesting a surface at that depth (Table 2). It is also possible that deviations in these values at the top of the profile reflect the influence of the Horus Ash. While Ni can be used to denote organic accumulations, it does not show any association with other soil features or elemental species in this profile (Figure 5).

Changes in the intensity of aggradation and degradation over time have welded the horizons of the lower sedimentary package to upper part of the profile to create the thickest paleosol for this particular paleocatena(Table 2; Figure 5, 6b). The summit position is the most stable and heavily leached along this paleocatena as indicated by CIW and $\frac{Ba}{Sr}$, as well as deep root penetration and highly developed soil fabric (Tables 2 and 8, Figure 5). The ratio of $\frac{Ba}{Sr}$ in this profile is less than two (the value for most rocks and soils) and, although the degree of leaching is highest in the summit profile, this suggests minimal leaching overall and semi-arid to arid climate conditions (Figure 5) (Birkeland, 1999; Sheldon and Tabor, 2009). However this paleosol did not experience

aridity to the point that salts were accumulated, as there is no salinization in this or any other profile. All salinization values are less than 1, which suggests that there is at least enough movement of water through the profile to dissolve and transport salts (Figure 5). The weathering indices, $\frac{\sum BASES}{Al_2O_3}$ and CIW, indicate translocation in the upper part of the profile and are not influenced by clayeyness and parent material in the upper 50 – 60 cm of the profile (Figure 5). The hydrolysis and movement of bases in the upper profile are slight, but they do occur, driving the trend of $\frac{CaO}{Al_2O_3}$ and influencing calculated climofunctions (Table 5).

There is more α-cristobalite, which is a by-product of the early stages of weathering of silica-rich volcanic materials, in the summit profile than either of the other two geomorphic positions (Clayton and Rex, 1971) (Figure 7). This is due to the increased surface stability and associated leaching and hydrolysis at the summit position, which would allow for the in-situ alteration of volcanic materials (Birkeland, 1999). This also explains the lower amounts of gypsum in the summit profile than in either of the other two landscape positions (Figure 8) (Birkeland, 1999). In arid environments solutes, such as calcium, are removed from the upland by groundwater, and re-precipitate in lower geomorphic positions as calcite and gypsum (Birkeland, 1999). Relative intensity of pedogenesis throughout the summit profile is consistent with the predicted stability and relatively high development of the summit position compared to other positions in the paleocatena (Table 2; Figure 2) (Birkeland 1999).

4.1.2 Shoulder

The shoulder profile consists of two sedimentary packages, which represent exhumed material deposited before the downcutting event (Figures 5 and 9). The highly erosive nature of the shoulder position is truncating the active pedogenic surface faster than soil formation can occur (Birkeland, 1999). There are no root traces in the shoulder profile (Table 3).

Clayeyness ($\frac{Al_2O_3}{SiO_2}$) does not correlate with grain size in the shoulder profile, but instead reflects overall sedimentary packages (Figure 5). Paleofertility ($\frac{P_2O_5}{TiO_2}$), Cu, and Ni all represent the accumulation of organic matter in this profile, although they are diminished at the top due to erosional truncation at this position. Spikes in Cu and Ni values at ~30 cm depth and Ni at ~60 cm depth suggest that these were exposed surfaces, or zones of accumulation, which were at least somewhat stable in the history of this paleosol (Figure 5). ($\frac{P_2O_5}{TiO_2}$) shows very little variation at the top of the profile as the original paleosol surface was likely removed via truncation (Figure 5). The ratio of $\frac{Ba}{Sr}$ in this profile never reaches a value of 2, which indicates very weak pedogenesis with minimal leaching, although there is a high at the top of the profile and ~60 cm depth coinciding with the previous land surfaces (Figure 5). The weathering indicies, $\frac{\sum BASES}{Al_2O_3}$ and CIW, are all erratic and reflect differences in parent material, especially above the boundary between the two sedimentary packages (Figure 5). The hydrolysis and movement of bases in this profile, if present, are too erratic to detect (Table 6). There is no salinization in this or any other profile among the paleocatena, which suggests that

there is sufficient movement of water through the profile to dissolve and transport salts (Figure 5).

There is minimal α-cristobalite in the shoulder profile due to the low surface stability caused by continuous erosional truncation, as well as more gypsum in the shoulder profile than in the summit, suggesting that Ca was moved down slope along the paleocatena (Figures 7, and 9) (Birkeland, 1999). This is consistent with the chemical and mineralogical changes predicted for shoulder positions (Birkeland, 1999).

4.1.3 Backslope

The backslope profile also encompasses two main sedimentary sequences, although its sedimentary history is more complex (Table 4; Figure 5). The micromorphology of the lower zone of pedogenic development directly beneath the Horus Ash layer is similar to the summit profile, although the backslope profile is composed of finer materials(Table 4; Figures 6f, and 9). The materials above the Horus Ash along the backslope are predominantly finer than those below (Table 4; Figures 6g, and 9). As the valley went from a degradational to an aggradational regime, the position that was once the backslope became more fluvially influenced as the valley below it was filled with sediment (Figure 9). This backslope eventually became a footslope or toeslope as deposition filled the valley (Figure 9). The cumulic paleovalley backfill is the result of multiple depositional episodes, as shown by the various levels at which pedogenic features exist within the upper sedimentary sequence of the backslope profile (Table 4; Figure 5). Root traces in the backslope profile are larger, and penetrate less deeply than those in the summit profile (Table 4; Figures 5 and 6e). This may indicate more poorly

drained conditions in the backslope, but without evidence of hydromorphy the nature of the drainage is uncertain.

Clayeyness, ($\frac{Al_2O_3}{SiO_2}$), approximates grain size in the backslope profile, generally decreasing upsection, while also decreasing below ~110 cm. Combined with Paleofertility ($\frac{P_2O_5}{TiO_2}$), Cu, and Ni, which all represent the presence of organic matter, the cumulic, fluvial additions to the backslope profile are evident as multiple aggradational surfaces (Figure 5). The ratio of $\frac{Ba}{Sr}$ in this profile never reaches a value of 2, which suggests very weak pedogenesis with minimal leaching (Sheldon and Tabor, 2009). There is no salinization in this profile, which suggests sufficient movement of water through the profile to dissolve and transport salts, but not enough to flush the accumulations of gypsum (Figures 5 and 8). The extremely low value for leaching at ~60 cm, corresponds to highs in Cu and Ni and may represent a rapid accumulation of sediment, reducing the apparent leaching to near zero (Figure 5). The weathering indices, $\frac{\sum BASES}{Al_2O_3}$ and CIW, however, indicate an accumulation of bases in the upper 80 cm of the backslope profile (Figure 5). The accumulation of these bases is due to the throughflow of water laterally through the catena, driving the trend of $\frac{CaO}{Al_2O_3}$ and influencing calculated climofunctions (Table 6; Figure 2).

There is very little α-cristobalite in the backslope profile due to the low surface stability caused by frequent colluvial and fluvial additions (Figures 8, and 9). There is also more gypsum in the backslope profile than in the summit, suggesting the throughflow effect of water transporting solutes along the paleocatena (Figures 2 and 7) (Birkeland, 1999). This gypsum is not diagenetic because of its segregation by

paleotopography (Figure 7). However, the XRD sample used for the backslope profile came from the top of the profile, so it is not contemporaneous with the other samples, but does illustrate the general behavior of solutes at the backslope position.

4.2 Classification

USDA Soil Taxonomy (Soil Survey Staff, 2010), although intended for descriptions of modern soils, is useful when applied to paleosols. It can help to restrict possible modern analogues and put a paleosol in a more constrained pedogenic context. However, certain diagnostic soil features do not preserve well in lithified paleosols, so USDA classification of paleosols is partially dependent on inference and can be highly subjective. In many cases, classification can only proceed to the subgroup or great group level. This is due to a lack of diagnostic features, or good analogues, and is done to reduce the possibility of inappropriate assumptions.

The summit profile is actually two paleosols formed on distinct sedimentary packages, which were welded together during downcutting of the Horus paleovalley. Howevr, I will consider it as one soil for classification purposes as the welding represents a gradual zone and not a distinct pedogenic boundary (Table 2; Figures 5 and 9). The presence of pedogenic carbonate and gypsum, as well as the low level of leaching, indicate a semi-arid climate (Table 2; Figures 5, 6c, and 8). This paleosol has a Btk horizon at ~20 cm depth. Adjusting for compaction to 70% of original thickness (Terry, 2001), this does not meet the requirement to be an Aridisol. The juxtaposition of the shallow Btk horizon with the deep root penetration may indicate this soil is the product of a decrease in precipitation over time (Table 2; Figure 5). Given the high base saturation,

and paleofertility, as well as the depth of root penetration and root morphology, this soil is likely a Mollisol, although there is no way to truly determine original color and the percentage of carbon (Table 2; Figures 5 and 6c). Given the presence of gypsum and pedogenic carbonate, and the lack of salinization, as well as the presence of an argillic (Btk) horizon, I classify the summit paleosol as an Argiustoll (Table 2; Figures 5, 6c and 8) (Soil Survey Staff, 2010).

The shoulder profile has no B horizon and thus no epipedon, therefore this paleosol must be an Entisol. Although the sediments that compromise the shoulder profile beneath the Horus layer were deposited by fluvial activity prior to downcutting, fluvial influence did not contribute to the genesis of this profile, therefore this is an Orthent. Given the presence of gypsum, as well as the lack of salinization in the profile, I classify the shoulder paleosol as an Ustorthent (Table 3; Figures 5 and 8) (Soil Survey Staff, 2010).

The backslope profile is actually two paleosols, which will be considered separately due to differences in pedogenic features. The backslope profile above the Horus Ashfall has no B horizon and was influenced by fluvial action of the backfilling Horus paleovalley while pedogenesis was altering the sediment. The backslope profile below the Horus Ashfall has a B horizon and its micromorphology shows the same type of pedogenic fabric to the summit profile, although it developed on fluvial, paleovalley fill sediments (Figure 9). The paleosols in this profile are interpreted to have an ustic soil moisture class based on the presence of calcium carbonate rhizoliths and gypsum, as well as the lack of salinization (Table 4; Figures 5, 6e, and 8). Based on the physiographic position of the backslope profile above the Horus Ashfall, combined with its cumulic

nature, as represented by multiple fluvial depositional packages, I classify the upper portion of the backslope profile as a Pachic Ustifluvent (Soil Survey Staff, 2010). The backslope profile below the Horus Ashfall is micromorphologically similar to the summit profile, although it is thinner and less well developed. Although it has the necessary base saturation, it is not thick enough, nor well enough developed to be a Mollisol (Table 4; Figure 5). I classify the lower portion of the backslope profile as a Haplustept (Soil Survey Staff, 2010).

4.3 Climofunctions

It was hypothesized that the paleosols along this paleocatena would differ in their geochemistry based on topographic effects, and that those differences would be sufficient to affect paleoenvironmental reconstructions based on climofunctions. It was expected that the climofunctions for the summit would indicate wetter and cooler conditions in the summit relative to the lower positions. This hypothesis is not supported. Although the values obtained from the climofunctions do differ from one another in the ways predicted by our current understanding of soil catenary relationships, differences in geochemistry were insufficient to compromise the application of climofunctions in this particular paleoenvironmental setting.

Solutes were stripped from the well-drained upland position and precipitated in the lowland areas, producing higher than unaltered parent material concentrations and altering the trends of $\frac{CaO}{Al_2O_3}$ and CIW to suggest anomalously low rates of weathering in lowland positions (Figure 5), as well as enriching lower positions in gypsum at the expense of the summit (Figure 7). If bases were actually accumulating in the backslope

Table 7. Relationship between landscape position and soil features.

Profile	Summit	Shoulder	Backslope
Apparent leaching	Highest	Low	Lowest
CIW	Highest	Low	Lowest
Mineralogy	More cristobalite	More gypsum	More gypsum
Root traces	Small, many	None	Large
Pedogenic fabric	Lattisepic	Isotic	Isotic over lattisepic
Sedimentary stability	Stable	Degrading, truncated	Aggrading, cumulic
Classification	Argiustoll	Ustorthent	Pachic Ustifluvent over Haplustept
Climofunctions	Cooler, wetter	None	Warmer, drier
T(s)	9.9 ± 4.4	NA	10.2 ± 4.4
T(c)	9.8 ± 0.6	NA	10.0 ± 0.6
P(BASES)	694 ± 235	NA	636 ± 235
P(CIW)	759 ± 181	NA	609 ± 181

'NA' indicates lack of climofunction data due to paleosol having no B horizon.

profile due to *in situ* pedogenesis, pedogenic carbonate glaebules would be evident (Table 4; Figure 6e, f, g). However, no glaebules were found. The values of CIW correspond to the alteration of common silicate minerals. A CIW value of 50 represents unweathered microcline, and as the value becomes higher, more altered mineral species are indicated, up to the CIW value of 100 which indicates kaolinite (Sheldon and Tabor,

2009). CIW values in the upper 70 cm of the backslope profile are consistently less than 50, which would suggest precipitation of $CaCO_3$ and $CaSO_4$. This could also indicate a change in parent material from felsic to mafic, but that is not the case in this section.

4.4 Implications

With our current state of understanding of modern soil geomorphology and influences of topography, climofunctions lack the required resolution when dealing with paleotopography. Interpretations based on macromorphology, micromorphology, and clay mineralogy are reliable and follow predicted trends in modern soil systems. The difference between the upland and lowland positions in all climofunctions used in this study falls within the error inherent in the respective equations, and they are thus not statistically significant. Although chemical segregation is noted between upland and lowland soil profiles, as predicted by modern soil geomorphology, errors of the MAP climofunctions in particular are very large, and would regard the difference in modern rainfall between Eastern and Western Nebraska as non-significant, although this difference represents a definitive boundary between soil forming regimes (udic vs. ustic soil moisture class). Climofunction equations could be significant with a more robust quantification specifically tailored to common paleopedologic scenarios. The current climofunction equations are derived using data from the modern Great Plains (Marbut, 1935). Equations specifically tailored to common regimes of the five primary soil forming factors of Jenny (1961) would be better suited for paleoclimate reconstructions of paleosols. This kind of specificity is necessary for a complete understanding of soils as a system.

Local scale resolution is important for accurate reconstruction of paleoenvironments as the basin scale is not fine enough to track the dynamic nature of soils and how they change in response to regimes of climatic perturbation. It is at the local/hillslope scale that major transitions in terrestrial ecology begin. The riparian partitioning of plant communities is a common ecological scenario which is driven by geomorphologically mediated changes in hydrology. This partitioning furthers the differentiation of soils along a hillslope.

Without knowledge of their paleotopographic association, these paleosols would seem to have formed in environments with potentially different climatic conditions. The macromorphology, geochemistry, and clay mineralogy suggest different soil environments. The micromorphology suggests different intensities of weathering and pedogenesis, as well as differences in ecology (Table 8). The sedimentology and mineralogy of individual profiles indicate very different depositional environments. These indicators are misleading by themselves, but are predicted by a catenary understanding of soil development as a dynamic function of the landscape.

CHAPTER 5

CONCLUSIONS

The processes of erosion, deposition, and the through flow of water change in a predictable way along modern landscapes as a result of changes in slope, base level, and back-and-forth transitions from convexity to concavity. Soils forming on different landscape positions, even though they are adjacent to one another, develop strikingly different morphologies, and without knowledge of their topographic association can be interpreted as having formed under vastly different pedogenic settings.

Reconstruction of paleoenvironments in and around the Eocene-Oligocene Boundary has significant implications for the temporal and spatial evolution of Cenozoic paleoecology. Paleosols along an Oligocene topographic transect were found to differ in morphology, chemistry, and mineralogy due to their physiographic position (Table 8). Macromorphology and micromorphology are the most difficult for topographic effects to alter, because they are derived from physical processes within the soil. Those physical processes can govern some of the chemical evolution of a soil, but geochemistry, as well as clay mineralogy, are most susceptible to the influence of catenary differentiation. In this study, evidence for catenary differentiation was observed within each of the methods used to evaluate paleopedology.

Leaching and weathering, as indicated by CIW and $\frac{\mathrm{Ba}}{\mathrm{Sr}}$, were low for this paleocatena. The summit position was the most pedogenically developed overall, with the greatest amount of leaching and weathering. High stability allowed for deep root penetration, which welded previous surfaces into one large and complex paleosol, and

promoted greater production of cristobalite due to volcaniclastic weathering. The shoulder position expressed only incipient soil formation due to constant erosion, although there was more gypsum in the shoulder position due to flushing of Ca^{2+} from the summit.

The backslope position was more complex. Before the Horus Ashfall the backslope was moderately well developed, but afterward cumulic additions from the upland began to outpace pedogenesis. This increase in local sedimentation rate decreased relative pedogenic development. There was more gypsum, as well as MgO and CaO in the backslope due to the throughflow effect of water transporting solutes downslope. These differences are predicted by catenary understanding of modern soil development.

Although downslope flow of water accumulated MgO and CaO in lower topographic positions, the accumulation did not affect the results of paleoclimate reconstruction using paleosol climofunctions. Climofunction calculations from the composition of B horizons in the summit and backslope paleosols were not significantly different. All climofunction values fall within the range of error, which would be expected over the limited extent of the study area, but other paleosol features suggest differences in the order and great group level of soil classification.

REFERENCES

Aubry, M. and Bord, D., 2009, Reshuffling the cards in the photic zone at the Eocene/Oligocene boundary, in Koeberl, C. and Montanari, A. eds., The Late Eocene Earth: hothouse, icehouse, and impacts: Geological Society of America Special Paper 452, p. 279-302.

Billups, K., 2008, A tale of two climates, Nature Geoscience, v. 1 p. 294 – 295.

Birkeland, P. W., 1999, Soils and Geomorphology, Oxford University Press, 430 p.

Clayton, R. N., and Rex, R. W., 1971, Clays and Clay Minerals, v. 19, p. 229 – 238.

Conacher, A. J. and Dalrymple, J. B., 1977, The nine unit landsurface model: an approach to pedogeomorphic research, Geoderma, v. 18, p. 1-154.

Evanoff, E., Prothero, D. R., and Lander, R. H., 1992, Eocene-Oligocene climatic change in North America: the White River Formation near Douglas, east-central Wyoming, in Prothero, D. R., and Berggren, W. A., eds., Eocene-Oligocene climatic and biotic evolution, Princeton University Press, p. 116 – 130.

Franklin and Marshall, 2010, http:// http://www.fandm.edu/earth-and-environment/precision-and-accuracy

Gerrard, J., 1992, Soil geomorphology: an integration of pedology and geomorphology, London, Chapman and Hall, 273 p.

Grandstaff, D. E., and Terry Jr., D. O., 2009, Rare earth element composition of Paleogene vertebrate fossils from Toadstool Geologic Park, Nebraska, USA, Applied Geochemistry, v. 24, n. 4, p. 733 – 745.

Gregory, S. V., Swanson, F. J., McKee, W. A., and Cummins, K. W., 1991, An ecosystem perspective of riparian zones: focus on links between land and water, BioScience, v. 41, n. 8, p. 540 – 551.

Griffis, N. and Terry, D. O., 2010, Vertical changes in paleosol morphology within the White River Sequence at Flagstaff Rim, Wyoming: implications for paleoclimatic change leading up to the Eocene-Oligocene transition, Geological Society of America Abstracts with Programs, v. 42, n. 3, p. 42.

Harnois, L., 1988, The CIW index: a new chemical index of weathering, Sedimentary Geology, v. 55, p. 319 – 322.

Hilgen, F. J., and Kuiper, K. F., 2009, A critical evaluation of the numerical age of the Eocene-Oligocene boundary in Koeberl, C. and Montanari, A. eds., The Late Eocene Earth: hothouse, icehouse, and impacts: Geological Society of America Special Paper 452, p. 139 – 148.

Jenny, H. J., 1961, Derivation of state factor equations of soils and ecosystems in Soil Science Society Proceedings, p. 385 – 388.

Kahnmann, J. A., Seaman III, J., and Driese, S. G., 2008, Evaluating trace elements as paleoclimate indicators: multivariate statistical analysis of Late Mississippian Pennington Formation paleosols, Kentucky, USA, Journal of Geology, v. 116, p. 254 – 268.

Kennett, J. P., 1977, Cenozoic evolution of Antarctic glaciation, the Circum-Antarctic Ocean, and their impact on global paleoceanography, Journal of Geophysical Research, v.82, n. 27, p. 3843 – 3860.

Lagabrielle, Y., Godderis, Y., Donnadieu, Y., Malavielle, J., and Suarez, M., 2009, The tectonic history of Drake Passage and its possible impacts on global climate, Earth and Planetary Science Letters, v. 279, p. 197 – 211.

LaGarry, H. E., 1998, Lithostratigraphic revision and redescription of the Brule Formation (White River Group) of Northwestern Nebraska in Terry Jr., D. O., LaGarry, H. E., and Hunt Jr., R. M., eds., Depositional environments, lithostratigraphy, and biostratigraphy of the White River and Arikaree Groups (Late Eocene to Early Miocene, North America): Geological Society of America Special Paper 325, p. 63 – 91.

Larson, E. E., and Evanoff, E., 1998, Tephrostratigraphy and source of the tuffs of the White River Sequence in Terry Jr., D. O., LaGarry, H. E., and Hunt Jr., R. M., eds., Depositional environments, lithostratigraphy, and biostratigraphy of the White River and Arikaree Groups (Late Eocene to Early Miocene, North America): Geological Society of America Special Paper 325, p. 1 – 14.

Leopold, E. B., and Clay-Poole, S. T., 2001, Florissant leaf and pollen floras of Colorado compared: climatic implications, Proceedings of the Denver Museum of Natural History, v. 4, p. 17 – 69.

Marbut, C. F., 1935, Atlas of American Agriculture Part III, soils of the United States, United States Department of Agriculture Advance Sheets 8, Washington (D.C.), U.S. Government Printing Office, 98 p.

Maynard, J. B., 1992, Chemistry of modern soils as a guide to interpreting Precambrian paleosols, Journal of Geology, v. 100, p. 279 – 289.

McCoy, M., 2002, Controls on paleosol morphology in a basin wide marker bed in the Scenic Member of the Brule Formation, Badlands National Park, South Dakota, [M.S. Thesis]: Philadelphia, Temple University, 77 p.

Metzger, C. A., Terry Jr., D. O., and Grandstaff, D. E., 2004, Effect of paleosol formation on rare earth element signatures in fossil bone, Journal of Geology, v. 32, n. 6, p. 497 – 500.

Miller K. G., Fairbanks, R. G., and Mountain, G. S., 1987, Tertiary oxygen isotope synthesis, sea level history, and continental margin erosion, Paleoceanography, v. 2, n. 1, p. 1 – 19.

Milne, G., 1935, Some suggested units of classification and mapping particularly for East African soils, Soil Research, v. 4, p. 183 – 198.

Moore, D. M., and Reynolds, R. C., 1997, X-ray diffraction and the identification and analysis of clay minerals, Oxford University Press,

Munsell Color, 2000, Munsell soil color chart: Baltimore, Md., 22 p.

Nahon, D., 1991, Introduction to the petrology of soils and chemical weathering, Wiley, 313 p.

Nesbitt, H. W., and Young, G. M., 1982, Early proterozoic climates and plate motions inferred from major element chemistry of lutites, Nature, v. 299, p. 715 – 717.

Nordt, L., Orozs, M., Driese, S., and Tubbs, J., 2006, Vertisol carbonate properties in relation to mean annual precipitation: implications for paleoprecipitation estimates, Journal of Geology, v. 114, p. 501 – 510.

Prochnow, S.J., Nordt, L.C., Atchley, S.C., and Hudec, M.R., 2005, Multi-proxy paleosol

evidence for middle and late Triassic climate trends in eastern Utah, Palaeogeography, Palaeoclimatology, Palaeoecology, v. 232, p. 53–72.

Prothero, D. R., and Heaton, T. H., 1996, Faunal stability during the Early Oligocene climate crash, Paleogeography, Paleoclimatology, Paleoecology, v. 127, p. 257 – 283.

Prothero, D. R., and Whittlesey, K. E., 1998, Magnetic stratigraphy and biostratigraphy of the Orellan and Whitneyan land-mammal "ages" in the White River Group in Terry Jr., D. O., LaGarry, H. E., and Hunt Jr., R. M., eds., Depositional environments, lithostratigraphy, and biostratigraphy of the White River and Arikaree Groups (Late Eocene to Early Miocene, North America): Geological Society of America Special Paper 325, p. 39 – 62.

Retallack, G. J., 1983, A paleopedological approach to the interpretation of terrestrial sedimentary rocks: The mid-Tertiary fossil soils of Badlands National Park, South Dakota, Geological Society of America Bulletin, v. 94, n. 7, p. 823 – 840.

Retallack, G. J., 1992, Paleosols and change in climate and vegetation across the Eocene-Oligocene boundary in Prothero, D.R., Berggren, W.A. (Eds.), Eocene–Oligocene Climatic and Biotic Evolution. Princeton Univ. Press, Princeton, NJ, p. 116– 130.

Retallack, G. J., 2005, Pedogenic carbonate proxies for amount and seasonality of precipitation in paleosols, Journal of Geology, v. 33, n. 4, p. 333 – 336.

Retallack, G.J., 2007, Cenezoic paleoclimate on land in North America: The Journal of Geology, v. 115, p. 271-294.

Retallack, G. J., Wynn, J. G., and Fremd, T. J., 2004, Glacial-interglacial–scale paleoclimatic change without large ice sheets in the Oligocene of central Oregon, Journal of Geology, v. 32, n. 4, p. 297 – 300.

Sahy, D., Fischer, A., Terry, D.O., Condon, D., and Kuiper, K, 2010, Radio-Isotopic dating of volcanic ash layers from the White River Group, Wyoming and Nebraska, GSA Rocky Mountain Sections Abstracts with Programs, Rapid City, South Dakota, Abstract.

Schultz, C.B., and Stout, T.M., 1955, Classification of Oligocene sediments of Nebraska: Bulletin of the University of Nebraska State Museum, v. 4, p. 17-52.

Sheldon, N. D., 2006, Abrupt chemical weathering increase across the Permian-Triassic boundary, Paleogeography, Paleoclimatology, Paleoecology, v. 231, p. 315 – 321.

Sheldon, N. D., 2009, Nonmarine records of climatic change across the Eocene-Oligocene transition in Koeberl, C. and Montanari, A. eds., The Late Eocene Earth: hothouse, icehouse, and impacts: Geological Society of America Special Paper 452, p. 241 – 248.

Sheldon, N. D., Mitchel, R. L., Collinson, M. E., and Hooker, J. J., 2009, Eocene-Oligocene transition paleomagnetic and paleoenvironmental record from the Isle of Wight (UK) in Koeberl, C. and Montanari, A. eds., The Late Eocene Earth: hothouse, icehouse, and impacts: Geological Society of America Special Paper 452, p. 249 – 260.

Sheldon, N. D., and Retallack, G. J., 2004, Regional paleoprecipitation records from the Late Eocene and Oligocene of North America, The Journal of Geology, v. 112, p. 487 – 494.

Sheldon, N. D., Retallack, G. J., and Tanaka, S., 2002, Geochemical climofunctions from North American soils and application to paleosols across the Eocene-Oligocene boundary in Oregon, The Journal of Geology, v. 110, p. 687 – 696.

Sheldon, N. D., and Tabor, N. J., 2009, Quantitative paleoenvironmental and paleoclimatic reconstruction using paleosols, Earth Science Reviews, v. 95, p. 1 – 52.

Soil Survey Staff, 2010, Keys to soil taxonomy, 11th ed., eds.: Unites States Department of Agriculture, p. 346.

Stinchcomb, G. E., 2007, Paleosols and stratigraphy of the Scenic-Poleslide Member boundary, Early Oligocene Brule Formation, White River Group, Badlands National Park, South Dakota, USA, [M.S. Thesis]: Philadelphia, Temple University, 103 p.

Terry, Jr., D.O., 1998, Lithostratigraphic revision and correlation of the lower part of the White River Group: South Dakota to Nebraska: Geological Society of America Special paper 325, p. 15-35.

Terry, Jr., D. O., 2001, Paleopedology of the Chadron Formation of Northwestern Nebraska: implications for paleoclimatic change in the North American midcontinent across the Eocene-Oligocene boundary, Paleogeography, Paleoclimatology, Palaeoecology, v. 168, p. 1 – 38.

Terry, Jr., D. and Evans, J., 1994, Pedogenesis and paleoclimatic implications of the Chamberlain Pass Formation, Basal White River Group, Bad Lands of South Dakota: Journal of Sedimentary Geology, v. 110, p 197-215.

Terry, Jr., D.O., and LaGarry, H., 1998, The Big Cottonwood Creek Member: A new member of the Chadron Formation in northwestern Nebraska: Geological Society of America Special paper 325, p. 117-141

Uhl, D., Klotz, S., Traiser, C., Thiel, C., Utescher, T., Kowalski, E., and Dilcher, D., 2007, Cenozoic paleotemperatures and leaf physiognomy: a European perspective. Palaeogeography, Palaeoclimatology, Palaeoecology, v. 248, p. 24–31.

Utescher, T., and Mosbrugger, V., 2007, Eocene vegetation patterns reconstructed from plant diversity: a global perspective. Palaeogeography, Palaeoclimatology, Palaeoecology, v. 247, p. 243–271.

Wolfe, J.A., 1978, A paleobotanical interpretation of Tertiary climates in the northern hemisphere. American Scientist, v. 66, p. 694-703.

Zachos, J., Pagani, M., Sloan, L., Thomas, E., and Billups, K., 2001, Trends, rhythms, and aberrations in global climate 65 MA to present: Science, v. 292, p. 686-693.

Zanazzi, A., Kohn, M. J., McFadden, B. J., and Terry, Jr., D. O., 2007, Large temperature drop across the Eocene-Oligocene transition in central North America, Nature, v. 445, p. 639 – 642.

Zanazzi, A., Kohn, M. J., and Terry, Jr., D. O., 2009, Biostratigraphy and paleoclimatology of the Eocene-Oligocene boundary section at Toadstool Park, northwestern Nebraska, USA, in Koeberl, C. and Montanari, A. eds., The Late

Eocene Earth: hothouse, icehouse, and impacts: Geological Society of America Special Paper 452, p. 1 – 18.

APPENDIX

Appendix A. X-ray fluorescence instrument error

Element	Standard Error (±)	% Relative Standard Deviation
SiO_2	0.226 %	0.45
TiO_2	0.006 %	0.47
AL_2O_3	0.06 %	0.33
MgO	0.015 %	0.3
CaO	0.02 %	0.25
Na_2O	0.01 %	0.25
K_2O	0.006 %	0.55
P_2O_5	0.01 %	1.7
Sr	1.7 ppm	0.2
Y	0.2 ppm	0.6
Zr	0.6 ppm	0.5
Ni	1.5 ppm	2.5
Cr	11.3 ppm	12.6
Nb	0.12 ppm	1.3
Cu	2 ppm	2.6
Zn	1.15 ppm	1.4
Ba	8.5 ppm	1.5

Franklin and Marshall (2010).

Appendix B. Major element geochemistry in weight percent of oxides

Sample depth	SiO_2	TiO_2	Al_2O_3	MgO	CaO	Na_2O	K_2O	P_2O_5	Total
(Su) -10 cm	69.31	0.52	12.65	2.97	4.69	0.86	3.09	0.25	99.8
(Su) -20 cm	69.4	0.66	14.2	2.61	3.04	1.48	3.05	0.26	99.6
(Su) -30 cm	69.13	0.74	15.2	2.72	2.39	1.6	3.25	0.16	99.67
(Su) -40 cm	67.43	0.78	15.69	2.67	2.4	1.66	3.31	0.13	99.4
(Su) -50 cm	67	0.78	15.65	2.68	2.86	1.66	3.27	0.17	99.45
(Su) -60 cm	70.18	0.53	13.31	2.45	4.29	1.4	2.76	0.17	99.44
(Su) -70 cm	69.75	0.53	13.66	2.48	4.2	1.43	2.91	0.21	99.52
(Su) -80 cm	69.98	0.51	13.48	2.46	4.42	1.42	2.81	0.16	99.34
(Su) -90 cm	69.67	0.54	14.36	2.56	3.8	1.48	3.05	0.14	99.68
(Su) -100 cm	69.71	0.55	14.82	2.62	3.28	1.52	3.11	0.13	99.96
(Su) -110 cm	69.62	0.55	14.66	2.56	3.36	1.53	3.2	0.21	99.81
(Su) -120 cm	69.74	0.56	14.97	2.64	2.83	1.53	3.27	0.12	99.74
(Su) -130 cm	69.69	0.58	15.24	2.67	2.65	1.52	3.25	0.13	100.16

Appendix B. (continued)

Sample depth	SiO_2	TiO_2	Al_2O_3	MgO	CaO	Na_2O	K_2O	P_2O_5	Total
(Su) -140 cm	69.13	0.59	15.24	2.69	2.65	1.55	3.35	0.13	99.77
(Su) -150 cm	69.01	0.59	15.03	2.61	2.64	1.57	3.44	0.12	99.5
(Su) -160 cm	69.28	0.59	15.19	2.62	2.38	1.57	3.54	0.12	99.71
(Su) -170 cm	68.81	0.59	15.29	2.68	2.31	1.56	3.5	0.12	99.32
(Su) -180 cm	69.06	0.58	14.97	2.71	2.52	1.53	3.47	0.14	99.43
(Su) -190 cm	69.5	0.55	13.77	2.59	3.93	1.33	3.3	0.17	99.55
(Su) -200 cm	69.48	0.55	13.38	2.44	4.72	1.36	3.19	0.19	99.62
(Su) -210 cm	69.75	0.62	13.76	2.28	3.77	1.62	3.2	0.2	99.62
(Sh) -10 cm	68.38	0.59	14.72	2.63	4.29	1.65	2.82	0.15	99.43
(Sh) -20 cm	66.67	0.55	14.4	2.65	6.87	1.5	2.72	0.13	99.67
(Sh) -30 cm	68.4	0.56	15.46	2.97	3.18	1.5	2.95	0.13	99.58
(Sh) -40 cm	67.74	0.57	14.86	2.8	4.83	1.53	2.8	0.13	99.55
(Sh) -50 cm	68.22	0.55	15.61	3.03	3.03	1.49	2.93	0.11	99.53
(Sh) -60 cm	68.65	0.56	15.47	2.89	2.92	1.55	3.03	0.13	99.57
(Sh) -70 cm	68.98	0.56	13.93	3.03	3.67	1.02	3.12	0.17	99.52
(Sh) -80 cm	68.37	0.56	14.21	2.75	4.6	1.38	2.96	0.17	99.47
(Sh) -90 cm	69.62	0.59	14.48	2.52	3.24	1.63	2.87	0.16	99.34
(Sh) -100 cm	69.76	0.57	13.85	2.27	4.6	1.74	2.7	0.18	99.66
(Sh) -110 cm	69.7	0.57	13.94	2.25	4.57	1.73	2.68	0.18	99.44
(Bs) -10 cm	66.97	0.57	14.05	3.2	4.88	1.07	3.32	0.18	99.45
(Bs) -20 cm	63.73	0.53	13.38	3.02	9.67	0.77	3.32	0.17	99.52
(Bs) -30 cm	64.15	0.53	13.37	2.96	9.76	0.78	3.3	0.17	99.83
(Bs) -40 cm	64.26	0.52	13	2.96	9.77	0.78	3.18	0.17	99.7
(Bs) -50 cm	65.6	0.54	13.04	3.03	7.79	0.83	3.26	0.19	99.21
(Bs) -60 cm	66.17	0.56	13.75	3.1	6.74	0.83	3.43	0.19	100.1
(Bs) -70 cm	63.73	0.54	13.94	3.01	9.4	1.18	2.97	0.18	99.5
(Bs) -80 cm	66.18	0.55	13.67	3.13	6.48	1.08	3.14	0.24	99.49
(Bs) -90 cm	69.43	0.58	15.2	2.8	2.91	1.6	2.71	0.12	99.42
(Bs) -100 cm	68.52	0.56	15.18	2.82	4.06	1.58	2.69	0.13	99.53
(Bs) -110 cm	68.24	0.41	16	3.51	3.99	1.22	2.67	0.14	99.96
(Bs) -120 cm	66.77	0.54	14.56	2.6	7.18	1.55	2.66	0.23	99.96
(Bs) -130 cm	67.64	0.58	14.47	2.58	5.23	1.58	2.82	0.2	99.32
(Bs) -140 cm	67.64	0.55	14.13	2.47	6.33	1.56	2.68	0.19	99.52

Appendix C. Minor element geochemistry in parts per million

Sample depth	Sr	Ni	Cr	Nb	Cu	Zn	Ba
(Su) -10 cm	216	20	46	12.7	20	94	457
(Su) -20 cm	407	16	41	13.9	25	76	792
(Su) -30 cm	474	17	41	14.7	25	84	951
(Su) -40 cm	550	16	39	15.2	24	82	1155
(Su) -50 cm	557	16	41	15.5	25	83	1158
(Su) -60 cm	423	15	35	12.4	19	70	797
(Su) -70 cm	438	15	41	12.9	18	75	948
(Su) -80 cm	432	16	36	12.7	18	73	842
(Su) -90 cm	485	16	37	13.7	15	74	976
(Su) -100 cm	478	16	48	14.2	16	76	1070
(Su) -110 cm	503	16	35	14.8	21	77	1099
(Su) -120 cm	482	16	43	13.3	14	70	1056
(Su) -130 cm	483	17	39	14.5	16	80	1041
(Su) -140 cm	501	16	39	13.4	17	74	1111
(Su) -150 cm	515	16	42	13.5	14	72	1167
(Su) -160 cm	510	17	40	14.8	18	84	1180
(Su) -170 cm	514	18	47	15.3	17	83	1138
(Su) -180 cm	489	18	42	16.1	18	87	1094
(Su) -190 cm	380	19	50	13.5	17	77	756
(Su) -200 cm	374	19	42	13.6	17	75	712
(Su) -210 cm	461	17	49	13.8	16	70	874
(Sh) -10 cm	437	15	53	16	14	66	834
(Sh) -20 cm	424	15	40	15.7	17	70	753
(Sh) -30 cm	428	17	44	15.8	19	74	757
(Sh) -40 cm	418	16	40	14.4	14	70	837
(Sh) -50 cm	431	17	42	15.1	15	77	849
(Sh) -60 cm	481	17	39	16.3	18	79	959
(Sh) -70 cm	239	20	45	14.4	18	89	503
(Sh) -80 cm	386	18	41	15.1	18	81	790
(Sh) -90 cm	452	16	48	14.2	15	67	897
(Sh) -100 cm	488	15	52	14.4	16	66	912
(Sh) -110 cm	489	15	50	14	14	62	929
(Bs) -10 cm	279	21	42	13.8	23	93	581
(Bs) -20 cm	188	21	41	12.3	22	93	362
(Bs) -30 cm	195	20	39	11.7	21	84	353
(Bs) -40 cm	179	19	38	10.9	20	83	330
(Bs) -50 cm	188	20	39	12	26	88	355

Appendix C. (continued)

Sample depth	Sr	Ni	Cr	Nb	Cu	Zn	Ba
(Bs) -60 cm	286	22	45	13	27	97	362
(Bs) -70 cm	315	20	37	13.8	18	84	606
(Bs) -80 cm	254	20	41	13.5	21	84	504
(Bs) -90 cm	410	14	53	18.3	12	63	768
(Bs) -100 cm	401	15	41	18.9	11	61	765
(Bs) -110 cm	296	17	28	23.1	8	64	568
(Bs) -120 cm	429	15	41	21.6	12	72	856
(Bs) -130 cm	433	15	46	15.4	12	65	870
(Bs) -140 cm	430	16	40	14.5	15	66	825